Benchmarking of DFT methods using experimental free energies and volumes of activation for the cycloaddition of alkynes to cuboidal Mo_3S_4 clusters

Journal:	*International Journal of Quantum Chemistry*
Manuscript ID	QUA-2020-0098.R2
Wiley - Manuscript type:	Full Paper
Date Submitted by the Author:	12-May-2020
Complete List of Authors:	Pedrajas, Elena; Universidad de Cadiz Facultad de Ciencias, Departamento de Ciencia de los Materiales e Ingeniería Metalúrgica y Química Inorgánica Pino-Chamorro, José Ángel; Universidad de Cadiz Facultad de Ciencias, Departamento de Ciencia de los Materiales e Ingeniería Metalúrgica y Química Inorgánica Ferrer, Montserrat; Universidad de Barcelona Centro de Recursos para el Aprendizaje y la Investigación Biblioteca de Física y Química, Departament de Química Inorgànica i Orgànica, Secció de Química Inorgànica Fernández-Trujillo Rey, María Jesús; Universidad de Cadiz Facultad de Ciencias, Departamento de Ciencia de los Materiales e Ingeniería Metalúrgica y Química Inorgánica Llusar, Rosa; Universitat Jaume I, Departament de Química Física i Analítica Martínez, Manuel; Universidad de Barcelona Facultad de Biologia, Departament de Química Inorgànica i Orgànica, Secció de Química Inorgànica Basallote, Manuel; Universidad de Cadiz Facultad de Ciencias, Departamento de Ciencia de los Materiales e Ingeniería Metalúrgica y Química Inorgánica Algarra, Andrés; Universidad de Cadiz Facultad de Ciencias, Departamento de Ciencia de los Materiales e Ingeniería Metalúrgica y Química Inorgánica
Keywords:	Benchmarking, DFT methods, Metal clusters, Cycloaddition reaction, Activation volume

International Journal of QUANTUM CHEMISTRY WWW.Q-CHEM.ORG FULL PAPER

Benchmarking of DFT methods using experimental free energies and volumes of activation for the cycloaddition of alkynes to cuboidal Mo_3S_4 clusters

Elena Pedrajas,[1,2] José A. Pino-Chamorro,[1] Montserrat Ferrer,[3] M. Jesús Fernández-Trujillo,[1] Rosa Llusar,[2] Manuel Martínez,[3] Manuel G. Basallote,[1] Andrés G. Algarra[1]

Correspondence to: Andrés G. Algarra (E-mail: *andres.algarra@uca.es*)

[1] *Elena Pedrajas, José A. Pino-Chamorro, M. Jesús Fernández-Trujillo, Manuel G. Basallote, Andrés G. Algarra*
Departamento de Ciencia de los Materiales e Ingeniería Metalúrgica y Química Inorgánica, Universidad de Cádiz, Apartado 40, Puerto Real, 11510 Cádiz, Spain
[2] *Elena Pedrajas, Rosa Llusar*
Departament de Química Física i Analítica, Universitat Jaume I, Av. Sos Baynat s/n, 12071 Castelló, Spain
[3] *Montserrat Ferrer, Manuel Martínez*
Departament de Química Inorgànica i Orgànica, Secció de Química Inorgànica, Universitat de Barcelona, Martí i Franquès 1-11, E-08028 Barcelona, Spain

ABSTRACT

Herein, the kinetics of the concerted [3+2] cycloaddition reaction between the $[Mo_3(\mu_3\text{-}S)(\mu\text{-}S)_3Cl_3(dmen)_3]^+$ (dmen=*N,N*'-dimethyl-ethylenediamine) ([**1**]$^+$) cluster and various alkynes to form dithiolene derivatives is thoroughly studied, with measurements at different temperatures and pressures allowing the determination of the free energies and volumes of activation. These parameters, together with the available single crystal X-ray diffraction structures are employed to test a number of commonly used DFT methods from across the Jacob's ladder, as well as the effects associated with the size of the basis sets, the way in which solvent effects are taken into account, or the inclusion of dispersion effects. All in all, a protocol that leads to average deviations between experimental and computed $\Delta V^{\#}$ and $\Delta G^{\#}$ values similar to the uncertainty of the experimental measurements is obtained.

Introduction

Theory is expected to provide answers to the many questions related with the mechanism of chemical reactions. This goal requires of accurate computational methods, and for that purpose an adequate estimation of the activation parameters is critical. In this sense, recent analyses have highlighted that obtaining reliable and predictive mechanistic insight from modelling remains challenging.[1-2] As the kinetic and mechanistic features of reactions are best evaluated by using activation parameters, an adequate refinement of computational methods for evaluating them is highly desired.

Given the difficulties of the current methodology to separate enthalpic and entropic contributions, estimation of the experimental activation free energies is surely the best way to test the performance of computational methods. The activation volume, another activation parameter typically less used because of its higher experimental demands, is also fundamental for obtaining an adequate mechanistic picture of reactions, and so the development of adequate procedures for obtaining accurate computational estimations is also pursued. In the present work we tested the capability of the most commonly used DFT methods to model the activation parameters of

a series of concerted reactions between Mo/S species and alkynes.

Mo^{IV} combines with sulfur to generate robust clusters with a $[Mo_3(\mu_3\text{-}S)(\mu\text{-}S)_3]^{4+}$ core.[3-4] These structures thus feature two types of sulfur ligands, with each metal centre being coordinated to the capping (μ_3-S) and two bridging (μ-S) ligands (see Scheme 1). Moreover, each metal centre features a distorted octahedral geometry if the Mo-Mo bonds are ignored, and therefore three additional coordination sites are normally occupied by mono- and/or polydentate ligands. Besides the reactivity associated to the Mo(IV) centres and its outer coordination environment,[5] the three bridging (μ-S) ligands provide important reactivity paths. In fact, two main processes are known to occur at these sulphur sites: a) incorporation of a second metal (M') to form heterometallic $[Mo_3M'S_4]^{4+}$ clusters[6]; b) alkyne insertion to produce dithiolene adducts, as shown in Scheme 1.[7] According to previous findings, such insertion takes place through a concerted [3+2] cycloaddition process between a $[Mo(\mu\text{-}S)_2]$ cluster moiety and the two *sp* carbon atoms of the alkyne, as illustrated in Scheme 1 (see also Figure S3).[7]

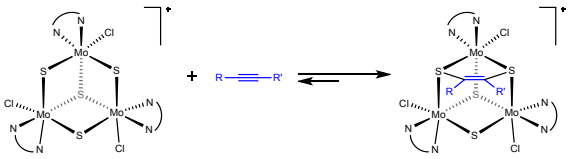

Scheme 1. [3+2] cycloaddition reaction between [**1**]$^+$ and alkynes (dmen ligands represented as N^N).

From a computational point of view, although DFT results have been used to explain all the observed trends in reactivity, we have found inconsistencies associated with errors of up to 5-6 kcal/mol in the predicted free energies.[8-10] In this manuscript we have taken advantage of the clean reaction between the [**1**]$^+$ cluster and some alkynes, dimethylacetylene dicarboxylate (dmad) and phenylacetylene (PhA), to identify which of the commonly used computational approaches produce the most accurate results. To do so, not only have we used the interatomic distances calculated from their single crystal X-ray diffraction structures, but also free energy barriers and activation volumes kinetically determined. In this way, an optimised computational strategy has been developed that yields estimations of activation parameters that are typically within the standard deviation of the experimental determinations. Furthermore, the protocol was tested on other [3+2] cycloaddition reactions of $[Mo_3S_4]^{4+}$ cuboidal clusters with similar results, thus highlighting its versatility. Thus, the conclusions of this work constitute an excellent starting point towards future calculations on catalytic processes involving these clusters.

Additionally, it is worth noting that such clusters are important in relation to Group-VI transition metal dichalcogenides (TMDs), a class of materials thoroughly studied nowadays due to their ability to catalyse the Hydrogen evolution reaction (HER).[11] The location of the catalytic active sites of these materials is however still under debate, and in this sense, the use of homogeneous analogues able to mimic their structure has been cleverly used by some researchers to shed light into this dilemma.[12] Among those model species, $[Mo_3(\mu_3\text{-}S)(\mu\text{-}S)_3]^{4+}$ clusters share structural similarities with the basal planes of MoS_2,[13] and therefore any improvement in their computational characterisation will reverberate in a better understanding of HER catalysts.

Methods

Chemical substances

The cluster $[Mo_3S_4Cl_3(dmen)_3](BF_4)$, [**1**]$(BF_4)$, was prepared according to literature procedures.[14-15] All other chemicals were

International Journal of QUANTUM CHEMISTRY WWW.Q-CHEM.ORG FULL PAPER

reagent grade commercially available and were used as received.

Kinetic experiments

Ambient pressure kinetic experiments were carried out using an Applied Photophysics SX-18MV stopped-flow spectrophotometer provided with a PDA1 photodiode array detector, and with a Cary 50 Bio UV-Vis spectrophotometer for conventional measures. All experiments were carried out at the desired temperatures in acetonitrile solution by mixing a stock solution of the cluster ($2–5 \times 10^{-4}$ M) with another solution containing the alkyne in a concentration range large enough (0.01–0.050 M) to ensure pseudo-first order conditions of alkyne excess. Some experiments at two different cluster concentrations were also carried out to confirm the first order dependence of the observed rate constants on its concentration. Runs at variable high pressure were conducted with the same procedures, but using the pressurising systems and cells described previously.[16]

All time-resolved data were collected as full (300-1000 nm) spectra and treated with the standard Specfit or ReactLab Kinetics software.[17-18] Observed rate constants were obtained from the full time-resolved spectral changes or alternatively at the wavelength were a maximum change was observed (*ca.* 400 or 900 nm). For the vast majority of the runs the changes agreed with the operation of an A→B single exponential equation when pseudo-first order conditions applied, and were fitted accordingly. In cases where a drift of the absorbance values was observed, the data were fitted to two consecutive exponentials but the values derived for the second rate constants showed erratic changes and were disregarded.

Computational details

All calculations were performed with Gaussian 09, Revision D.01.[19] Optimisations were carried out in the gas phase without any symmetry constraint, and employed an integration grid obtained with 99 radial shells and 590 angular points per shell centred on each atom, which is denoted as "ultrafine" in Gaussian 09. Vibrational frequencies were computed using the harmonic oscillator approximation on all optimised geometries at 1 atm and 298.15 K. This served to characterise them as either minima or transition states, as well as to obtain the thermal and entropic corrections required to further calculate free energy differences. The connection of transition states with the corresponding reactants and products was confirmed via intrinsic reaction coordinate (IRC) calculations[20-21] and subsequent optimisation to minima. Unless otherwise stated, BS1 was employed for optimisation purposes and BS2 to obtain improved energetic values via single-point calculations. A summary of how each basis set system is constructed is included in Table 1. BS1 uses the Stuttgart RECPs and corresponding basis sets to describe the Mo and S centres,[22] with added polarisation on the latter (ζ= 0.503),[23] whereas the Pople style 6-31G(d,p) basis set is used for all other atoms (Cl, N, O, C, H). Mo and S centres are described similarly in BS2, which only differs from BS1 in that the remaining atoms are modelled using the 6-311+G(2d,2p) basis set. Nevertheless, given that previous DFT studies on reactions involving Mo centres have shown a significant dependence of results on the quality of the basis set,[24-25] additional optimisations and/or single-point calculations were performed with the basis set systems indicated in Table 1. This includes common basis set systems such as BS3, invoked in Gaussian software by using the SDD

Table 1. Summary of basis set systems used in this work.

Basis set system	Mo centres	S centres	Cl, N, O, C and H centres
BS1	SDD/ECP[a]	SDD/ECP[a] + Pol[b]	6-31G(d,p)
BS2	SDD/ECP[a]	SDD/ECP[a] + Pol[b]	6-311+G(2d,2p)
BS3	SDD/ECP[a]	D95	
BS4	cc-pVDZ-PP[c]	cc-pVTZ[d]	cc-pVDZ[e]
BS5	Def2-TZVP[f]	Def2-TZVP[f]	Def2-TZVP[f]

[a] SDD/ECP = Stuttgart / Dresden ECP, see Ref. 22. [b] Added polarisation function (ζ= 0.503), see Ref. 23. [c] Ref. 27. [d] Ref. 28. [e] Ref. 29. [f] Ref. 26.

command, a combination of Dunning's correlation consistent basis sets and effective core potentials in BS4, or the triple-ζ valence basis set including polarisation functions Def2-TZVP optimised by Weigend and Ahlrichs.[26]

A number of popular density functionals across the Jacob's ladder[30] were employed and they are included in Table 2. On each case, both optimisations and subsequent single-point calculations were carried out with the same density functional. The latter single-point calculations at the DFT/BS2 level included the effects of the solvent (acetonitrile) using either the IEFPCM[31] (abbreviated PCM) or the SMD[32] approaches.

Dispersion effects were taken into account in different ways. No additional correction was applied to those functionals that already include these in some way, such as B97D3, wB97XD. For the remaining functionals, both Grimme's D3(0) and D3(BJ) dispersion corrections were computed as single-point corrections whenever possible. Note that for the M06 series only the D3(0) correction could be applied due to the lack of Becke-Johnson parameters. In addition, in some cases Grimme's D3(0) and D3(BJ) corrections were included self-consistently in the optimisation procedure, leading to the BP86D3(BJ), B3LYPD3(BJ), PBE0D3(0) and PBE0D3(BJ) combinations. Finally, no dispersion corrections were computed for the M11 functional.

A number of additional corrections were also considered in order to calculate activation free energies. Given that all reactions investigated take place in solution, a standard state of 1 M was employed. For that purpose, the quantity of R ln(24.46), 6.354 cal/mol·K, was subtracted from the raw entropies obtained from Gaussian 09 for each computed species.[33] Note that, in the present case, this subtraction results in a correction term of 1.89 kcal/mol for each species, which in turn leads to the same 1.89 kcal/mol energy decrease on the free energy barrier ($\Delta G^{\#}$) for the forward reaction between cluster and alkynes, with the correction cancelling out in the case of the reverse barrier.

Table 2. Summary of Exchange-Correlation Functionals used in this work.

Name	Type [a]	X [b]	Ref.
BP86	GGA	0	36-37
BP86D3(BJ) [c]	GGA+D	0	36-39
B97D3 [c]	GGA+D	0	40
TPSS	mGGA	0	41
M06-L	mGGA	0	42
TPSSh	GH-mGGA	10	43-44
B3LYP	GH-GGA	20	45
B3LYPD3(BJ) [c]	GH-GGA+D	20	45
PBE0	GH-GGA	25	46-47
PBE0D3(0) [c]	GH-GGA+D	25	38-39, 46-47
PBE0D3(BJ) [c]	GH-GGA+D	25	38-39, 46-47
M06	GH-mGGA	27	48
M06-2X	GH-mGGA	54	48
M06-HF	GH-mGGA	100	49
M11	RSH-mGGA	42.8-100	50
wB97XD [d]	RSH-GGA+D	22.2-100	51-52

[a] GGA = generalised-gradient approximation; +D = addition of molecular mechanic dispersion corrections; GH-GGA = global hybrid GGA, GGA plus some percentage of nonlocal HF exchange; mGGA = meta-GGA, GGA plus local kinetic energy density and some percentage of nonlocal HF exchange; RSH = range-separated hybrid. [b] X denotes de percentage of Hartree-Fock exchange. A single value indicates a local (X=0) or hybrid (X≠0) functional, whereas two values indicate X at short and long inter-electronic separations. [c] These functionals include Grimme's D3(BJ) correction, see Ref. 38-39. [d] This functional uses a version of Grimme's D2 dispersion correction.

On the other hand, the molecular symmetry of the species has an impact on their rotational entropy. All optimised species in this study were computed with C1 symmetry, and therefore the effect of symmetry was subsequently added to the free energy. This was carried out by including the term R ln(σ), where σ represents the symmetry number.[34-35] In particular, symmetry numbers of 3 and 2 were used for

International Journal of QUANTUM CHEMISTRY WWW.Q-CHEM.ORG FULL PAPER

cluster and alkynes, respectively, which led to contributions of 0.65 and 0.41 kcal/mol. A symmetry number of 1 was used for the transition states and dithiolene products, thus resulting in no additional correction for these species. As a result, this symmetry correction leads to a decrease of 1.06 kcal/mol on the free energy barrier for the forward reaction between cluster and alkyne.

All in all, the activation free energies reported in the text at a DFT2/BSX(solvent)//DFT1/BSY(gas) (X, Y= 1-5; solvent= PCM, SMD) level of theory are based on the electronic energies computed at the DFT2/BSX(solvent) level (note that in those cases in which DFT2 corresponds to a dispersion corrected functional, such dispersion correction is included in this term), and also include the free energy correction computed at the DFT1/BSY(gas) level, the standard state correction to change from 1 atm to 1 M, and the correction to account for the symmetry of the molecules. The molecular vdW volumes required to compute the $\Delta V^{\ddagger}$ values were obtained using the default Gaussian09 parameters for PCM and SMD solvation models, i.e. scaled (f = 1.1) UFF (Universal Force Field) and unscaled intrinsic atomic Coulomb radii, respectively.

A summary of the computed energies and vdW volumes for all optimized species is included in the Supporting Information, whereas their structures are available at the ioChem BD database,[53] where they can be accessed via https://doi.org/10.19061/iochem-bd-6-34.

Results and discussion

Kinetics of the reaction of [1]$^+$ with alkynes

The reaction of [**1**]$^+$ with an excess of various alkynes (adc, dmad, PhA, DPhA, PrA) was preliminary investigated (adc = acetylenedicarboxylic acid; PrA = propargyl alcohol; DPhA = diphenylacetylene; PrA = propargyl alcohol). While no reaction with DPhA was observed even after 4 days at 60 ºC, the reaction with PhA and PrA occurred in a few hours at room temperature, and in seconds

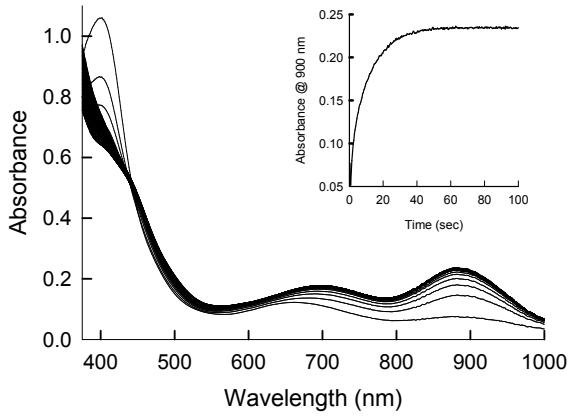

Figure 1. Typical spectral changes for the reaction of cluster [**1**]$^+$ with dmad in acetonitrile solution (25.0 ºC, [**1**]$^+$ = 4.57×10-4 M, [dmad] = 0.016 M).

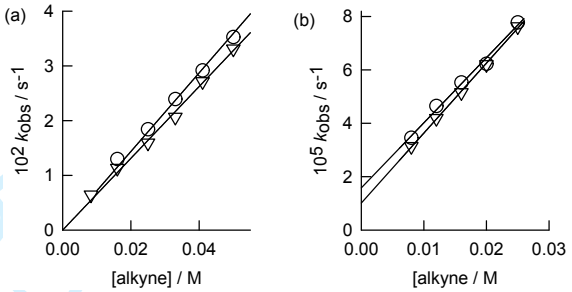

Figure 2. Representative plots of the dependence of the observed rate constants for the reaction of [**1**]$^+$ with different alkynes in acetonitrile solution at 25.0 ºC (a): dmad (circles) and adc (triangles); b): PhA (circles) and PrA (triangles).

when adc and dmad were used (the kinetics of the reaction with dmad at 25ºC has been previously reported).[13] The typical spectral changes observed for the reaction of [**1**]$^+$ with an excess of dmad in acetonitrile solution are shown in Figure 1. A significant change in the intensity of the bands at 400 and 660 nm is evident, as well as the appearance of a new band at 885 nm, which is a characteristic feature of the dithiolene addition products.[7]

Similar spectral changes are observed with the other alkynes, and in all cases they can be fitted

to a single exponential A→B model, i.e. no reaction intermediate build-ups in significant concentration during the cycloaddition process. The concentration dependence of the obtained pseudo-first order rate constants (k_{obs}, collected in Table S1 of the supporting information) are shown in Figure 2 for the different systems studied. Interestingly, the data show a non-zero intercept for the PhA and PrA alkyne systems, i.e. those showing the reactivity in the hours time scale, whereas the faster reacting activated dmad and adc alkynes feature a zero intercept. Such dependences can be explained by the rate law in eq 1, where k_+ and k_- correspond to the forward and reverse rate constants for the formation of the cycloaddition products in an equilibrium process. The equilibrium nature of the reactions with PhA and PrA is confirmed by the increasing magnitude of the absorbance changes when the alkyne concentration is increased. The reactions with dmad and adc can be considered to represent irreversible processes under the experimental conditions used. Table 3 collects the relevant kinetic parameters for all the systems studied (k_- and k_+) as well as the calculated equilibrium constants for the process ($^{calc}K_{eq} = k_+/k_-$).

$$k_{obs} = k_- + k_+ \cdot [\text{alkyne}] \qquad (1)$$

Table 3. Summary of kinetic and equilibrium parameters obtained for the reaction of [**1**]$^+$ with the different alkynes studied.[a]

Parameter	dmad	PhA	PrA	adc
$^{298}k_+/M^{-1}s^{-1}$	0.72(2)	$1.53(5)\cdot10^{-3}$	$2.62(4)\cdot10^{-3}$	0.65(1)
$^{298}k_-/s^{-1}$	-	$2.6(1)\cdot10^{-5}$	$1.01(7)\cdot10^{-5}$	
log $^{calc}K_{eq}$	-	2.51(6)	3.2(1)	

[a] Numbers in parenthesis are errors in the last significant digit.

The variation of the kinetic parameters with temperature and pressure were also determined for the PhA and dmad systems, as representatives of the two types of kinetic trends in Figure 2. Figure 3 shows the Eyring and lnk/P plots for the systems studied (see also Figures S1 and S2), whereas Table 4 collects the corresponding thermal and pressure activation parameters derived. The activation enthalpy for the cycloaddition (forward process) is lower in the case of dmad, and the negative activation entropies are, in both cases, in agreement with an ordering on going to the transition state, a fact that is also shown by the negative activation volumes in the non-polar, non-protic media used for the study (acetonitrile). For the reaction with PhA the data even allow for a comprehensive description of the reversible process. The activation parameters for the forward and backward reaction lead to a reasonable estimation of the corresponding thermodynamic ΔH_0 = 6.2 ± 2.6 kJ mol^{-1}, ΔS_0 = 33 ± 8 J K^{-1} mol^{-1}, and ΔV_0 = -18 ± 2 cm^3 mol^{-1}. It is important to note that the values indicate that the overall reaction is thermodynamically favoured (ΔG_0 <0), despite an unfavourable enthalpy term, due to its entropy changes.

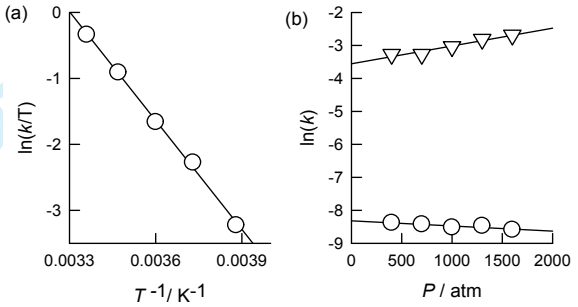

Figure 3. a) Eyring plot for the tempertaure dependence of the k_+ rate constant for the reaction of the [**1**]$^+$ cluster with dmad; b) ln(k) versus P plot for the k_+ (triangles) and k_-(circles) rate constants for the reaction of the [**1**]$^+$ cluster with PhA.

International Journal of QUANTUM CHEMISTRY WWW.Q-CHEM.ORG FULL PAPER

Table 4. Experimental activation parameters for the different reactions studied.[a]

Parameter	Reaction 1 PhA Forward	Reaction 2 PhA Reverse	Reaction 3 dmad Forward
$\Delta H^{\#}$/kcal mol^{-1}	19(1)	12(2)	9.9(1)
$\Delta S^{\#}$/cal K^{-1} mol^{-1}	-6(3)	-39(7)	-26.3(5)
$^{298}\Delta G^{\#}$/kcal mol^{-1}	21(1)	24(3)	17.7(2)
$\Delta V^{\#}$/cm^3 mol^{-1}	-14(2)	4(1)	-16(1)

[a] Numbers in parenthesis are errors in the last significant digit.

Table 5. For the optimisation of [**1**]$^+$ and [**1-dmad**]$^+$ with the PBE0 functional and various basis set systems, summary of mean unsigned errors (MUEs) with respect to their X-ray structures together with the number of resulting basis functions for each optimisation.

Basis set system	MUE [**1**]$^+$	MUE [**1-dmad**]$^+$	Basis functions for [**1**]$^+$/ [**1-dmad**]$^+$
BS1	0.010	0.009	658/828
BS2	0.011	0.009	1087/1411
BS3	0.034	0.036	495/607
BS4	0.014	0.017	811/981
BS5	0.018	0.018	1153/1499

Computational results on the reaction of [1]$^+$ with alkynes

The main purpose of this manuscript is to test which computational methodology is able to better model the previous experimental results. To do so, we have performed calculations aimed at determining not only the effect of the density functional, but also other important aspects such as the size of the basis set system, the inclusion of dispersion effects, or the way in which solvents effects are modelled.

Optimised structures

The X-ray diffraction structures of the cluster [**1**](BF_4) and the product of its reaction with dmad ([**1-dmad**]$_2$(Mo_6Cl_{14}) can be found in the literature.[13-14] These have been employed to determine which functional leads to the most accurate optimised structures when using the basis set system BS1. The results, listed in Tables S3 and S4, show that differences between optimised and experimental interatomic distances are small, i.e. each functional performs relatively similarly for both structures. As expected, common DFT methods not including dispersion effects such as BP86 and B3LYP systematically result in expanded structures, whereas those accounting for such effects lead to more compact structures.[54] This palliates the systematic overestimation of internuclear distances and reduces the general overestimation of bond lengths. The effect is clear for instance when comparing B3LYP and B3LYPD3(BJ) data. The different flavours of the Minnesota M06 family of functionals behave quite similarly, only showing a small improvement in the mean unsigned error MUE values with respect to BP86 and B3LYP.

From the data in Tables S3 and S4 it is difficult to determine a correlation between the percentage of HF exchange and the quality of the results, as dispersion effects seem to be much more important. In fact, among the two tested range-separated functionals, M11 and wB97XD, the latter gives generally better agreement with the experimental data probably because it contains a correction for dispersion effects. Interestingly, the best agreement (measured as the lowest MUE) within the functional selection herein is obtained for the PBE0 and its D3(0) and D3(BJ) dispersion-corrected versions. The PBE0 functional is known to give relatively accurate geometries for transition metal complexes,[55-59] nevertheless, it is quite surprising that: a) it gives lower MUE values than most dispersion-corrected functionals; b) the obtained MUE values are quite insensitive to the inclusion of dispersion corrections for this functional. The consequences of including solvent effects during the optimisation procedure have also been studied at the PBE0/BS1 level via PCM and SMD approaches (see the footnotes at Tables S3 and S4). Both for [**1**]$^+$ and [**1-dmad**]$^+$ this showed roughly no differences in terms of MUE

values when compared with the gas phase optimisations. On the contrary, the accuracy of the optimised structures strongly depends on the basis sets employed. The results of these calculations, carried out in the gas phase in combination with the PBE0 functional are included in Table 5. These show that the best agreement is obtained when BS1 and BS2 are employed, with only small differences between their MUE values. Given that BS1 and BS2 only differ in the way in which Cl, N, O, C, H atoms are modelled, with Pople style double- and triple-Z basis sets, respectively, it seems that the use of triple-Z basis set in the latter is not necessary to obtain accurate geometries. On the contrary, the accuracy decreases significantly when BS3 is employed, thus suggesting that the Dunning/Huzinaga full double zeta basis set is not appropriate for these optimisations. BS4 was selected on the basis of a recent computational assessment of DFT methods for Mo/W-mediated reactions.[25] As shown in Table 5, it leads to slightly larger MUE values than BS1, and a deeper analysis of the computed structures show that this is mostly originated by Mo–Mo and Mo–S distances ca. 0.01-0.02 Å shorter when BS3 is employed. The last basis set system tested, the polarised triple zeta valence def2-TZVP (BS5), leads to the largest number of basis functions among the tested basis set systems. Surprisingly, the PBE0/BS5 optimised structures are not as good as expected, an outcome probably related to the absence of pseudopotentials in the description of the Mo and S centres.

All in all, DFT calculations using the PBE0 functional and its dispersion corrected D3(0) and D3(BJ) versions in combination with the BS1 basis set constitutes the most accurate level of theory for optimisation purposes, leading to MUE values in the same range as the uncertainties of the X-ray diffraction determined interatomic distances.

Activation free energies

In spite of the fact that activation enthalpies and entropies have been obtained for the reaction of [**1**]$^+$ with dmad and adc in acetonitrile solution, herein we have focussed on the computation of the resulting Gibbs free energies in Table 4. This choice is based on the fact that the continuum solvation models employed herein, PCM and SMD, are constructed to calculate Gibbs free energies of solvation and do not provide direct information about separate enthalpies and entropies of solvation.[1] A wide range of density functionals have been tested and the results are included in Table S5. This allows comparing several common variables when trying to compute free energy barriers. For instance, regardless of how solvent effects are accounted for, the values obtained at levels of theory that do not include dispersion effects (entries 2, 5, 8, 11 and 14, Table S5) clearly overestimate the barriers for the forward reactions R1 and R3, whereas they underestimate the backward reaction R2, these discrepancies being in the range of 5-10 kcal/mol. As expected, inclusion of dispersion effects on the computation of the free energy barriers leads to significant decreases in the barriers of R1 and R3, in agreement with the fact that such processes involve a change in molecularity from 2 to 1. On the contrary, the effect is much smaller for the backward reaction in R2, where there is no change in molecularity.

Although the extent of the decrease on the $\Delta G^{\#}$ values for R1 and R3 differs between the D3(0) and D3(BJ) corrections, with the latter being slightly more pronounced, such corrections are found to be generally too large, leading to an underestimation of the barriers. This is clearly exemplified when comparing the barrier for reaction R1 (experimental $\Delta G^{\#}$ value of 20.8 kcal/mol, entry 1) with the computed values for the BP86 functional without and with added dispersion corrections (entries 2-4, Table S5). Focusing on the PCM results, these calculations overestimate the barrier by 5.3 kcal/mol when no dispersion effects are considered, whereas it becomes underestimated by 11.1 and 14.9 kcal/mol after inclusion of D3(0) and D3(BJ)

corrections, respectively. The B3LYP results (entry 11, Table S5) are worth highlighting at this point, as they are the worst among the selected methodologies, overestimating the barriers for R1 and R3 by more than 15 kcal/mol.

As previously shown for the BP86 functional, the best performer in terms of computed geometries (PBE0) also overestimates the barriers for R1 and R3 (entry 14, Table S5), and underestimates them when dispersion corrections are included (entries 15 and 16, Table S5). The obtained MUE values are however much better in this latter case, in part because the barrier for R2 is well accounted for in the three cases. The family of M06 functionals represent a nice opportunity to analyse how the %HF exchange affects the computed energies. These functionals include dispersion effects in some extent, and therefore the D3(0) corrections are smaller than for other functionals and lead to minor changes in the barriers. Focussing first on the non-D3(0) corrected values in entries 17, 19, 21 and 23 (Table S5), a clear correlation is easily spotted for the backward reaction R2, whose barrier linearly increases with the %HF exchange (R^2 = 0.98, see Figure S4) both for PCM and SMD solvent-corrected values). Among them, the data shows that the M06-2X variant is the best performer, being also worth noting that the addition of D3(0) correction improves the results up to MUE values of 1.3 and 2.5 kcal/mol for the PCM and SMD solvent corrected data, respectively (entry 22, Table S5). In relation to the %HF exchange subject, it is observed that the range-separated hybrids M11 and wB97XD do not lead to significant improvements (entries 26 and 27, Table S5). The non-dispersion-corrected M11 functional generally overestimates barriers whereas the dispersion corrected wB97XD underestimates them.

In order to test whether it is more appropriate to include dispersion corrections during the optimisation procedure or afterwards as a single-point correction, optimisations were initially performed employing the D3(BJ) corrected versions of BP86, B3LYP, and PBE0 functionals (entries 28-30, Table S5). As expected, comparison of the resulting free energy barriers with those in entries 4, 13, and 16 (Table S5) shows that this variable has relatively little effect on the outcome (differences smaller than 1 kcal/mol). For the sake of completeness, optimisations were also performed with the PBE0D3(0) functional (entry 31, Table S5), which again led to small differences with respect to the results obtained by adding the D3(0) correction to the PBE0 energies (entry 15, Table S5).

The way in which solvent effects are taken into account in the calculations also represent an important ingredient of the computational methodology. Herein we have only compared the well-known PCM and SMD approaches. In general, the data obtained with the latter model leads to a small improvement on the free energy barriers, although the effect depends on the specific level of theory. All in all, the data in Table S5 indicates that M06-2XD3(0)(BS2,PCM)/M06-2X(BS1) and PBE0D3(0)(BS2,SMD)/PBE0D3(0)(BS1) approaches, closely followed by PBE0D3(BJ)(BS2,SMD)/PBE0(BS1) and PBE0D3(BJ)(BS2,SMD)/PBE0D3(BJ)(BS1) are the most accurate among the tested ones. The dependence of the computed activation free energy barriers on the employed basis set system was analysed subsequently based on the PBE0/BS1 data (Table 6, entries 32-37). From the results in Table S5 it has already been shown that the D3(0) dispersion correction leads to lower MUE values than the D3(BJ) correction. The PBE0/BS1 structures have been used to confirm that this trend is independent of the employed basis set system, as clearly shown by the MUE values for entry 35 > 32, 36 > 33, and 37 > 34 in Table 6. Thus, focusing on the D3(0) corrected energies, the results indicate that indeed when BS1 (entry 32) is substituted by BS2 (entry 15) there is an average MUE improvement of ca. 3 kcal/mol. The BS4 basis set system (entry 33) generates MUE values between those of BS2 and BS1, and therefore its use is not justified. On the

contrary, despite its relatively poor performance for optimisation purposes, BS5 (entry 34) is found to be the best performer in terms of free energy barriers, in fact even better than BS2, reaching a MUE value of only 0.9 kcal/mol when combined with the SMD solvent model. Based on these findings, a similar basis set analysis was carried out on the PBE0D3(0)(BS1) optimised geometries (entries 38-40), which again showed that BS5 gives the best performance among the basis set systems tested for computing electronic energies. All in all, the results in this section indicate that the PBE0D3(0)(BS5,SMD)/PBE0D3(0)(BS1) level of theory allows achieving chemical accuracy (±1 kcal/mol), as it results in an MUE value of 0.7 kcal/mol, in the same range as the experimental errors.

Table 6. Based on the gas-phase optimised geometries at the PBE0/BS1 level of theory, effect of the basis set system on the computed activation free energies ($\Delta G^{\#}$, kcal/mol) for the forward and reverse reactions of [**1**]$^+$ with PhA (R1 and R2, respectively) and the forward reaction of [**1**]$^+$ with dmad (R3), and its mean unsigned error (MUE) with respect to the experimental values.

Entry	Level of theory	Solvent = PCM				Solvent = SMD			
		R1	**R2**	**R3**	***MUE***	**R1**	**R2**	**R3**	**MUE**
1	*Experimental*	*20.8*	*23.3*	*17.7*		*20.8*	*23.3*	*17.7*	
15	PBE0D3(0)(BS2,Solvent)/PBE0(BS1)	17.5	21.7	13.6	*3.0*	19.4	21.6	15.3	*1.8*
32	PBE0D3(0)(BS1,Solvent)/PBE0(BS1)	13.6	22.6	7.5	*6.0*	15.7	22.6	9.2	*4.8*
33	PBE0D3(0)(BS4,Solvent)/PBE0(BS1)	16.0	23.7	8.4	*4.8*	18.0	23.6	10.2	*3.5*
34	PBE0D3(0)(BS5,Solvent)/PBE0(BS1)	18.0	23.1	14.4	*2.1*	19.9	23.0	16.2	*0.9*
30	PBE0D3(BJ)(BS2,Solvent)/PBE0(BS1)	15.7	23.1	12.0	*3.7*	17.6	23.0	13.8	*2.5*
35	PBE0D3(BJ)(BS1,Solvent)/PBE0(BS1)	11.8	24.0	5.9	*7.2*	13.9	23.9	7.6	*5.9*
36	PBE0D3(BJ)(BS4,Solvent)/PBE0(BS1)	14.3	25.0	6.9	*6.3*	16.2	25.0	8.6	*5.1*
37	PBE0D3(BJ)(BS5,Solvent)/PBE0(BS1)	16.2	24.4	12.9	*3.5*	18.2	24.3	14.6	*2.2*
31	PBE0D3(0)(BS2,Solvent)/PBE0D3(0)(BS1)	17.8	21.8	13.6	*2.9*	19.9	21.8	15.3	*1.6*
38	PBE0D3(0)(BS1,Solvent)/PBE0D3(0)(BS1)	13.8	22.9	7.3	*5.9*	16.2	23.0	8.7	*4.6*
39	PBE0D3(0)(BS4,Solvent)/PBE0D3(0)(BS1)	16.3	24.0	8.3	*4.9*	18.5	24.0	9.8	*3.6*
40	PBE0D3(0)(BS5,Solvent)/PBE0D3(0)(BS1)	18.3	23.4	14.4	*2.0*	20.5	23.4	15.9	*0.7*

Activation volumes

The changes on the volumetric properties of a system along a reaction coordinate lead to the concept of volume profile. Similarly to energy profiles, within a volume profile it is possible to identify activation ($\Delta V^{\#}$) and reaction volumes (ΔV).[60] These magnitudes can be experimentally obtained by studying the effect of the pressure on the equilibrium and reaction constants of the process, as shown in Eq. 2 and 3. Moreover, within the framework of the transition state theory $\Delta V^{\#}$ and ΔV_R are related to the partial molar volumes of the products, transition state and reactants according to Eq. 4 and 5. Interestingly, such correlations have been exploited by computational chemists to obtain theoretical volume profiles, which can be used to predict the structure of transition states by comparing them with experimentally determined activation volumes.[61-62]

$$\Delta V = -RT\left(\frac{\delta \ln K}{\delta P}\right)_T \qquad (2)$$

International Journal of QUANTUM CHEMISTRY WWW.Q-CHEM.ORG FULL PAPER

$$\Delta V^{\#} = -RT\left(\frac{\delta \ln k}{\delta P}\right)_T \quad (3)$$

$$\Delta V^{\#} = V^{\#} - V_R \quad (4)$$

$$\Delta V = V_P - V_R \quad (5)$$

For the concerted [3+2] cycloaddition processes studied herein, it provides important information in support of the proposed mechanism. Thus, the empirical negative activation volumes obtained for the forward reactions are a clear indication of the contraction associated with the TS formation from the separated species, whereas the positive value obtained for the reverse process highlights the expansion undergone by the dithiolene adducts in order dissociate the alkyne moiety at the TS structure.

Interestingly, a specific computational method has been developed recently to study the effect of extreme pressure on reactions taking place in solution (XP-PCM),[63-64] ultimately allowing to compute ΔV_{reac} and $\Delta V^{\#}$ values.[65] Unfortunately, the range of pressures required to obtain $\Delta V^{\#}$ values via XP-PCM calculations goes from 0 to 8-10 GPa (1 GPa= 104 bar), i.e. two orders of magnitude larger than the highest pressures typically employed in the experiments (0-103 bar). Herein we have instead computed $\Delta V^{\ddagger}$ values based on the differences between the VdW volumes of transition state structures and reactants, a methodology successfully used for instance to study water exchange processes at transition metal complexes.[66-67]

The results so obtained, included in Table S6, are evidently very dependent on the way in which atomic radii are computed. By default, Gaussian09 uses different atomic radii models for the PCM and SMD approaches. Thus, while the scaled (f = 1.1) UFF is associated with PCM, an unscaled intrinsic atomic Coulomb radii is employed for SMD. The agreement between experimental and computed activation volumes in Table S6 is quite good in both cases. It is easily seen that the unscaled intrinsic atomic Coulomb radii leads to better results than the scaled UFF radii regardless of the employed DFT functional, with average MUE values of ca. 2 and 4 cm^3mol^{-1}, respectively. Again, the errors are larger for R1 and R3 than for R2, an effect likely to be associated with the change in molecularity of the former reactions. As noted above, the computed $\Delta V^{\#}$ values show little dependence with the DFT functional at which the optimisations were carried out. This is not surprising given that, although the employed density functional has obviously an impact on the resulting structures (see above), those geometrical differences are not significant enough to provoke major changes in the resulting molecular VdW surfaces. All in all, the computations in this section show that the SMD solvation model predicts $\Delta V^{\#}$ values that in average deviate by ca. 2 cm^3mol^{-1} with respect to the empirical ones, a value in fact very similar to the uncertainty of these empirical measurements.

Performance of the optimised procedure when modelling single temperature kinetic data

As the kinetics of reactions are often measured at a single temperature (typically 25ºC), we decided to test the performance of the optimised PBE0D3(0)(BS5, SMD)/PBE0D3(0)(BS1) protocol to model activation free energies obtained in this way. For this purpose, not only the reactions of [**1**]$^+$ with adc and PrA (see Table 3) were tested, but also previously reported data for the related $[Mo_3S_4(acac)_3(py)_3]^+$ cluster (acac = acetylacetonate; py = pyridine), for which differences between experimental and computed free energies of up to 5 kcal/mol have been noted.[9-10] Notably, from the reactions of [**1**]$^+$ a MUE value of 1.0 kcal/mol is obtained from the data in Table 7, thus indicating that the accuracy of the protocol remains relatively similar when tested on these alkynes. Furthermore, a similar MUE value results for the reactions of $[Mo_3S_4(acac)_3(py)_3]^+$ with alkynes, which therefore indicates that the protocol is also valid to study the reactivity of other clusters with a $[Mo_3(\mu_3\text{-}S)(\mu\text{-}S)_3]^{4+}$ core.

Table 7. Comparison of experimental and PBE0D3(0)(BS5,SMD)/PBE0D3(0)(BS1) computed values of $\Delta G^{\#}$ at 298 K for the [3+2] cycloaddition reaction of clusters $[\mathbf{1}]^+$ and $[Mo_3S_4(acac)_3(py)_3]^+$ with various alkynes[a] in acetonitrile.

Cluster	Alkyne	$\Delta G^{\#}$ at 298 K			
		Forward		Reverse	
		Exp.	DFT	Exp.	DFT
$[\mathbf{1}]^+$	adc	17.7	15.7		
	dmad	21.0	22.0	24.3	24.3
$[Mo_3S_4(acac)_3(py)_3]^+$	adc	16.2	14.4		
	dmad	15.4	15.5		
	btd	20.3	21.8		
	PrA	20.8	21.3	23.0	22.1
	PhA	20.8	20.0	22.3	20.9
	^{F}PhA	20.3	20.6		
	^{CF3}PhA	21.4	20.6		

[a] ^{F}PhA = 1-ethynyl-4-fluorobenzene; ^{CF3}PhA = 1-ethynyl-3,5-bis(trifluoromethyl)benzene.

Conclusions

Free energies ($\Delta G^{\#}$) and volumes ($\Delta V^{\#}$) of activation for the [3+2] cycloaddition reaction between the $[\mathbf{1}]^+$ cluster and two alkynes, dmad and PhA, have been determined based on a kinetic study at different temperatures and pressures. These data, together with the already reported interatomic distances for the X-ray diffraction structures of [**1**](BF_4) and [**1-dmad**]$_2$(Mo_6Cl_{14}) cluster salts have been subsequently employed to identify the most accurate computational protocol among those commonly employed for this purpose. To do so, different functionals and basis set systems have been studied and other important factors such as the inclusion of dispersion and solvent effects have also been taken into account. DFT calculations using the PBE0 functional and its dispersion corrected PBE0D3(0) version are the most accurate among the tested functionals, with similar performances in terms of interatomic distances, but the dispersion correction (either as single-point or included self-consistently in the optimisation procedure) has proven to be necessary in order to obtain accurate energetic data. Interestingly, little functional dependence was observed on the computation of activation volumes, a magnitude that is much more dependent on the way in which van der Waals surfaces are constructed. In general, the SMD solvation model was found to give better results than the PCM approach both in terms of $\Delta G^{\#}$ and $\Delta V^{\#}$. Basis sets were also found to lead to significant changes both in terms of computed geometries and $\Delta G^{\#}$ values; BS1 and BS5 lead to the most accurate results when employed for geometry optimisation and subsequent single-point calculations, respectively. All in all, we concluded that the PBE0D3(0)(BS5,SMD)/PBE0D3(0)(BS1) protocol represents a good compromise between accuracy and computational cost, leading to a MUE value of only 0.7 kcal/mol for the $\Delta G^{\#}$ values computed for the reactions between $[\mathbf{1}]^+$ and the dmad and PhA alkynes. Thus, the computational protocol developed herein demonstrates that accurate estimations of the activation free energies and volumes can be obtained with an adequate choice of the computational method. Moreover, its predictive capability for the reaction of a different cluster indicates that it can be extended to other systems when a fine computational analysis of the structure and reactivity of $[Mo_3S_4]^{4+}$ cuboidal clusters is required, and so we recommend its use.

Acknowledgments

Financial support from the Ministerio de Economía y Competitividad (CTQ2015-65707C2-1 and -2/FEDER and PGC2018-094417-B-I00) and Junta de Andalucía-FEDER (sol-201800106840-tra) is acknowledged.

Keywords: DFT benchmarking – 3+2 cycloaddition – Reaction mechanisms – Cluster compounds – Alkynes

Additional Supporting Information may be found in the online version of this article.

ORCID

Rosa Llusar https://orcid.org/0000-0002-3539-7269
Manuel Martínez https://orcid.org/0000-0002-6289-4586
Manuel G. Basallote https://orcid.org/0000-0002-1802-8699
Andrés G. Algarra https://orcid.org/0000-0002-5062-2858

References and Notes

1. J. N. Harvey, F. Himo, F. Maseras, L. Perrin, *ACS Catal.*, **2019**, *9*, 6803–6813.
2. S. Grimme, P. R. Schreiner, *Angew. Chem., Int. Ed.*, **2018**, *57*, 4170–4176.
3. I. S. Edward, M. Kazuko, In Transition Metal Sulfur Chemistry, American Chemical Society, **1996**.
4. A. L. Gushchin, Y. A. Laricheva, M. N. Sokolov, R. Llusar, *Russ. Chem. Rev.*, **2018**, *87*, 670–706.
5. A. G. Algarra, M. J. Fernández-Trujillo, M. G. Basallote, *Chem. Eur. J.*, **2012**, *18*, 5036–5046.
6. J. Á. Pino-Chamorro, Y. A. Laricheva, E. Guillamón, M. J. Fernández-Trujillo, A. G. Algarra, A. L. Gushchin, P. A. Abramov, E. Bustelo, R. Llusar, M. N. Sokolov, M. G. Basallote, *Inorg. Chem.* **2016**, *55*, 9912-9922.
7. A. G. Algarra, M. G. Basallote, in Advances in Inorganic Chemistry, eds. R. van Eldik, C. D. Hubbard, Academic Press, **2017**, vol. 70, pp. 311-342.
8. J. Á. Pino-Chamorro, A. G. Algarra, M. J. Fernández-Trujillo, R. Hernández-Molina, M. G. Basallote, *Inorg. Chem.* **2013**, *52*, 14334-14342.
9. J. Á. Pino-Chamorro, A. L. Gushchin, M. J. Fernández-Trujillo, R. Hernández-Molina, C. Vicent, A. G. Algarra, M. G. Basallote, *Chem. Eur. J.* **2015**, *21*, 2835-2844.
10. E. Bustelo, A. L. Gushchin, M. J. Fernández-Trujillo, M. G. Basallote, A. G. Algarra, *Chem. Eur. J.* **2015**, *21*, 14823-14833.
11. H. Wang, C. Li, P. Fang, Z. Zhang, J. Z. Zhang, *Chem. Soc. Rev.* **2018**, *47*, 6101-6127.
12. Z. Huang, W. Luo, L. Ma, M. Yu, X. Ren, M. He, S. Polen, K. Click, B. Garrett, J. Lu, K. Amine, C. Hadad, W. Chen, A. Asthagiri, Y. Wu, *Angew. Chem. Int. Ed.* **2015**, *54*, 15181-15185.
13. A. G. Algarra, E. Guillamón, J. Andrés, M. J. Fernández-Trujillo, E. Pedrajas, J. Á. Pino-Chamorro, R. Llusar, M. G. Basallote, *ACS Catal.*, **2018**, *8*, 7346-7350.
14. E. Pedrajas, I. Sorribes, K. Junge, M. Beller, R. Llusar, *ChemCatChem*, **2015**, *7*, 2675-2681.
15. E. Pedrajas, I. Sorribes, A. L. Gushchin, Y. A. Laricheva, K. Junge, M. Beller, R. Llusar, *ChemCatChem*, **2017**, *9*, 1128-1134.
16. M. Vázquez, M. Martínez, *Inorg. Chem.*, **2016**, *55*, 6731-6738.
17. R. A. Binstead, B. Jung, A. D. Zuberbühler, *SPECFIT-32*, Spectrum Software Associates, Chappel Hill, **2000**.
18. M. Maeder, P. King, *ReactLab*, JPlus Consulting Pty Ltd., East Fremantle, Australia, **2009**.
19. M. J. Frisch, G. W. Trucks, H. B. Schlegel, G. E. Scuseria, M. A. Robb, J. R. Cheeseman, G. Scalmani, V. Barone, B. Mennucci, G. A. Petersson, H. Nakatsuji, M. Caricato, X. Li, H. P. Hratchian, A. F. Izmaylov, J. Bloino, G. Zheng, J. L. Sonnenberg, M. Hada, M. Ehara, K. Toyota, R. Fukuda, J. Hasegawa, M. Ishida, T. Nakajima, Y. Honda, O. Kitao, H. Nakai, T. Vreven, J. A. Montgomery Jr., J. E. Peralta, F. Ogliaro, M. Bearpark, J. J. Heyd, E. Brothers, K. N. Kudin, V. N. Staroverov, R. Kobayashi, J. Normand, K. Raghavachari, A. Rendell, J. C. Burant, S. S. Iyengar, J. Tomasi, M. Cossi, N. Rega, J. M. Millam, M. Klene, J. E. Knox, J. B. Cross, V. Bakken, C. Adamo, J. Jaramillo, R. Gomperts, R. E. Stratmann, O. Yazyev, A. J. Austin, R. Cammi, C. Pomelli, J. W. Ochterski, R. L. Martin, K.

Morokuma, V. G. Zakrzewski, G. A. Voth, P. Salvador, J. J. Dannenberg, S. Dapprich, A. D. Daniels, O. Farkas, J. B. Foresman, J. V. Ortiz, J. Cioslowski, D. J. Fox, Gaussian 09, Revision D.01, *Gaussian, Inc.,* Wallingford CT **2009**.

20. C. Gonzalez, H. B. Schlegel, *J. Phys. Chem.*, **1990**, *94*, 5523-5527.
21. C. Gonzalez, H. B. Schlegel, *J. Phys. Chem.*, **1991**, *95*, 5853-5860.
22. D. Andrae, U. Haussermann, M. Dolg, H. Stoll, H. Preuss, *Theor. Chim. Acta*, **1990**, *77*, 123-141.
23. A. Hollwarth, M. Bohme, S. Dapprich, A. W. Ehlers, A. Gobbi, V. Jonas, K. F. Kohler, R. Stegmann, A. Veldkamp, G. Frenking, *Chem. Phys. Lett.*, **1993**, *208*, 237-240.
24. J.-L. Li, R. A. Mata, U. Ryde, *J. Chem. Theory Comput.*, **2013**, *9*, 1799-1807.
25. L. Hu, H. Chen, *J. Chem. Theory Comput.*, **2015**, *11*, 4601-4614.
26. F. Weigend, R. Ahlrichs, *Phys. Chem. Chem. Phys.*, **2005**, *7*, 3297-3305.
27. K. A. Peterson, D. Figgen, M. Dolg, H. Stoll, *J. Chem. Phys.*, **2007**, *126*, 124101.
28. A. K. Wilson, D. E. Woon, K. A. Peterson, T. H. Dunning, *J. Chem. Phys.*, **1999**, *110*, 7667-7676.
29. T. H. Dunning, *J. Chem. Phys.*, **1989**, *90*, 1007-1023.
30. J. P. Perdew, K. Schmidt, *AIP Conference Proceedings*, **2001**, *577*, 1-20.
31. J. Tomasi, B. Mennucci, R. Cammi, *Chem. Rev.*, **2005**, *105*, 2999-3093.
32. A. V. Marenich, C. J. Cramer, D. G. Truhlar, *J. Phys. Chem. B*, **2009**, *113*, 6378-6396.
33. J. H. Jensen, *Phys. Chem. Chem. Phys.*, **2015**, *17*, 12441-12451.
34. A. Fernández-Ramos, B. A. Ellingson, R. Meana-Pañeda, J. M. C. Marques, D. G. Truhlar, *Theo. Chem. Acc.*, **2007**, *118*, 813-826.
35. M. K. Gilson, K. K. Irikura, *J. Phys. Chem. B*, **2010**, **114**, 16304-16317.
36. A. D. Becke, *Phys. Rev. A*, **1988**, *38*, 3098.
37. J. P. Perdew, *Phys. Rev. B*, **1986**, *33*, 8822-8824.
38. S. Grimme, S. Ehrlich, L. Goerigk, *J. Comput. Chem.*, 2011, **32**, 1456-1465.
39. S. Grimme, J. Antony, S. Ehrlich, H. Krieg, *J. Chem. Phys.*, **2010**, *132*, 154104.
40. S. Grimme, *J. Comput. Chem.*, **2006**, *27*, 1787-1799.
41. J. Tao, J. P. Perdew, V. N. Staroverov, G. E. Scuseria, *Phys. Rev. Lett.*, **2003**, *91*, 146401.
42. Y. Zhao, D. G. Truhlar, *J. Chem. Phys.*, **2006**, *125*, 194101.
43. J. P. Perdew, J. Tao, V. N. Staroverov, G. E. Scuseria, *J. Chem. Phys.*, **2004**, *120*, 6898-6911.
44. J. P. Perdew, S. Kurth, A. Zupan, P. Blaha, *Phys. Rev. Lett.*, **1999**, *82*, 2544-2547.
45. A. D. Becke, *J. Chem. Phys.*, **1993**, *98*, 5648-5652.
46. J. P. Perdew, M. Ernzerhof, K. Burke, *J. Chem. Phys.*, **1996**, *105*, 9982-9985.
47. C. Adamo, V. Barone, *J. Chem. Phys.*, **1999**, *110*, 6158-6170.
48. Y. Zhao, D. G. Truhlar, *Theo. Chem. Acc.*, **2008**, *120*, 215-241.
49. Y. Zhao, D. G. Truhlar, *J. Phys. Chem. A*, **2006**, *110*, 13126-13130.
50. R. Peverati, D. G. Truhlar, *J. Phys. Chem. Lett.*, **2011**, *2*, 2810-2817.
51. J.-D. Chai, M. Head-Gordon, *Phys. Chem. Chem. Phys.*, **2008**, *10*, 6615-6620.
52. J.-D. Chai, M. Head-Gordon, *J. Chem. Phys.*, **2008**, *128*, 084106.
53. M. Álvarez-Moreno, C. de Graaf, N. López, F. Maseras, J. M. Poblet, C. Bo, *J. Chem. Inf. Model.*, **2015**, *55*, 95-103.
54. Y. Minenkov, Å. Singstad, G. Occhipinti, V. R. Jensen, *Dalton Trans.*, **2012**, *41*, 5526-5541.
55. R. Kang, H. Chen, S. Shaik, J. Yao, *J. Chem. Theory Comput.*, **2011**, *7*, 4002-4011.
56. M. P. Waller, H. Braun, N. Hojdis, M.

Bühl, *J. Chem. Theory Comput.*, **2007**, *3*, 2234-2242.
57. T. Sperger, I. A. Sanhueza, I. Kalvet, F. Schoenebeck, *Chem. Rev.*, **2015**, *115*, 9532-9586.
58. S. Zhao, Z.-H. Li, W.-N. Wang, Z.-P. Liu, K.-N. Fan, Y. Xie, H. F. Schaefer, *J. Chem. Phys.*, **2006**, *124*, 184102.
59. M. Bühl, C. Reimann, D. A. Pantazis, T. Bredow, F. Neese, *J. Chem. Theory Comput.*, **2008**, *4*, 1449-1459.
60. P. Muller, *Pure Appl. Chem.*, **1994**, *66*, 1077-1184.
61. H. Wiebe, M. Louwerse, N. Weinberg, *J. Chem. Phys.*, **2017**, *146*, 104104.
62. J. Spooner, H. Wiebe, M. Louwerse, B. Reader, N. Weinberg, *Can. J. Chem.* **2017**, *96*, 178-189.
63. R. Cammi, in Frontiers of Quantum Chemistry, Springer, Singapore, **2018**, pp. 273-288.
64. R. Cammi, C. Cappelli, B. Mennucci, J. Tomasi, *J. Chem. Phys.*, **2012**, *137*, 154112.
65. B. Chen, R. Hoffmann, R. Cammi, *Angew. Chem., Int. Ed.*, **2017**, *56*, 11126-11142.
66. M. Regueiro-Figueroa, D. Esteban-Gómez, R. Pujales-Paradela, L. Caneda-Martínez, A. de Blas, C. Platas-Iglesias, *Int. J. Quantum Chem.*, **2016**, *116*, 1388-1396.
67. C. D. Hubbard, R. van Eldik, *Inorg. Chim. Acta*, **2010**, *363*, 2357-2374.

GRAPHICAL ABSTRACT

AUTHOR NAMES: Elena Pedrajas, José A. Pino-Chamorro, Montserrat Ferrer, M. Jesús Fernández-Trujillo, Rosa Llusar, Manuel Martínez, Manuel G. Basallote, Andrés G. Algarra

TITLE: Benchmarking of DFT methods using experimental free energies and volumes of activation for the cycloaddition of alkynes to cuboidal Mo_3S_4 clusters

TEXT: Despite the pressure dependence of the rate of reactions allows obtaining its activation volume, this magnitude is rarely studied from a computational viewpoint. Along with their free energy barriers, herein the activation volume for the reaction of Mo_3S_4 clusters with alkynes is determined and subsequently used to obtain a computational protocol featuring average errors of 0.7 kcal mol^{-1} and 2 cm^3mol^{-1}, respectively.

GRAPHICAL ABSTRACT FIGURE:

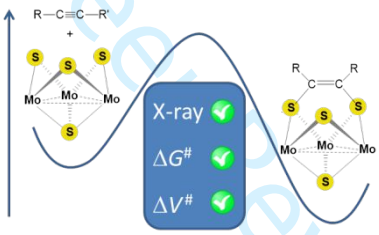

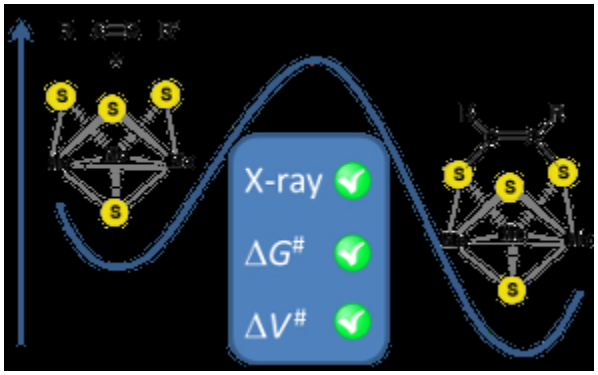

Image for the ToC

49x30mm (150 x 150 DPI)

Despite the pressure dependence of the rate of reactions allows obtaining its activation volume, this magnitude is rarely studied from a computational viewpoint. Along with their free energy barriers, herein the activation volume for the reaction of Mo_3S_4 clusters with alkynes is determined and subsequently used to obtain a computational protocol featuring average errors of 0.7 kcal mol^{-1} and 2 cm^3mol^{-1}, respectively.

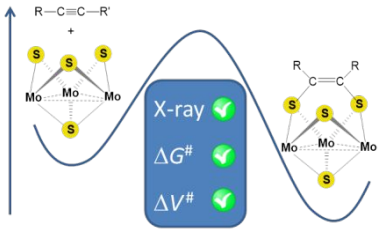

Supporting Information

Benchmarking of DFT methods using experimental free energies and volumes of activation for the cycloaddition of alkynes to cuboidal Mo_3S_4 clusters

Elena Pedrajas,[1,2] José A. Pino-Chamorro,[1] Montserrat Ferrer,[3] M. Jesús Fernández-Trujillo,[1] Rosa Llusar,[2] Manuel Martínez,[3] Manuel G. Basallote,[1] Andrés G. Algarra[1]

Departamento de Ciencia de los Materiales e Ingeniería Metalúrgica y Química Inorgánica, Universidad de Cádiz, Apartado 40, Puerto Real, 11510 Cádiz, Spain

[2] Departament de Química Física i Analítica, Universitat Jaume I, Av. Sos Baynat s/n, 12071 Castelló, Spain

[3] Departament de Química Inorgànica i Orgànica, Secció de Química Inorgànica, Universitat de Barcelona, Martí i Franquès 1-11, E-08028 Barcelona, Spain

Table of Contents **Pages**

Table S1.- Pseudo-first order rate constants obtained for the reaction of cluster $[\mathbf{1}]^+$ with different alkynes as a function of the alkyne concentration and temperature (at $4.57\text{x}10^{-4}$ M concentration of $[\mathbf{1}]^+$).

Alkyne	T /ºC	P /atm	$10^3\times$[Alkyne] /M	$10^3\times k_{obs}$ /s^{-1}
dmad	258	1	50	2.71
			67	3.00
			100	4.35
			133	5.60
	268	1	100	9.86
			133	13.30
			170	16.50
	278	1	67	13.00
			100	18.00
			133	26.00
	288	1	50	15.90
			67	23.40
			100	35.20
			133	51.10
			167	62.10
	298	1	8.3	8.40
			16	13.00
			25	18.00
			33	23.90
			41	29.00
			50	32.00
			67	43.40
			100	69.50
			133	92.10
			167	114.40
PhA	268	1	7.9	$9.77\text{x}10^{-3}$
			16	$1.23\text{x}10^{-2}$
			23	$1.50\text{x}10^{-2}$
			31	$1.70\text{x}10^{-2}$
			38	$1.87\text{x}10^{-5}$
	278	1	7.9	$1.78\text{x}10^{-2}$
			16	$2.58\text{x}10^{-2}$
			23	$2.80\text{x}10^{-2}$
			31	$3.51\text{x}10^{-2}$
			38	$3.72\text{x}10^{-2}$
	288	1	7.9	$3.14\text{x}10^{-2}$
			16	$4.00\text{x}10^{-2}$
			23	$4.85\text{x}10^{-2}$
			31	$5.58\text{x}10^{-2}$
			38	$6.38\text{x}10^{-2}$
	298	1	7.9	$3.73\text{x}10^{-2}$
			16	$5.12\text{x}10^{-2}$
			23	$6.10\text{x}10^{-2}$
			31	$7.20\text{x}10^{-2}$

			38	8.50×10^{-2}
	363		0.94	2.7×10^{-1}
			4.7	3.6×10^{-1}
			8.4	5.0×10^{-1}
			12	5.8×10^{-1}
			16	7.0×10^{-1}
PrA	298	1	8	3.13×10^{-2}
			12	4.18×10^{-2}
			16	5.15×10^{-2}
			20	6.20×10^{-2}
			25	7.62×10^{-2}
adc	298	1	8.3	6.40
adc			16	11.30
adc			25	15.92
adc			33	20.63
adc			41	27.13
adc			50	33.1

Table S2.- Second order rate constants obtained (typically errors of *ca.* 5%) for the reaction of cluster $[\mathbf{1}]^+$ with dmad and PhA as a function of the pressure.

Alkyne	*T* /ºC	[Alkyne] /M	*P* /atm	k_{obs} /s^{-1}	k_+ /M^{-1} s^{-1}	k_- /s^{-1}
dmad	298	0.10	250	7.1×10^{-2}	0.71	--
			300	7.1×10^{-2}	0.71	--
			450	7.7×10^{-2}	0.77	--
			600	9.0×10^{-2}	0.90	--
			750	10×10^{-2}	1.0	--
			900	11×10^{-2}	1.1	--
			1000	11×10^{-2}	1.1	--
			1050	12×10^{-2}	1.2	--
			1200	12×10^{-2}	1.2	--
			1350	15×10^{-2}	1.5	--
			1500	16×10^{-2}	1.6	--
PhA	363	0.0014	400	2.6×10^{-4}		
		0.0041		4.0×10^{-4}		
		0.012		7.1×10^{-4}		
		0.015		7.7×10^{-4}		
					3.8×10^{-2}	2.3×10^{-4}
		0.0014	700	2.8×10^{-4}		
		0.0041		3.8×10^{-4}		
		0.0095		5.7×10^{-4}		
		0.015		8.0×10^{-4}		
					3.8×10^{-2}	2.2×10^{-4}
		0.0014	1000	2.6×10^{-4}		
		0.0041		4.2×10^{-4}		
		0.012		7.5×10^{-4}		
		0.015		9.4×10^{-4}		
					4.8×10^{-2}	2.0×10^{-4}

		0.0014	1300	2.9×10^{-4}		
		0.0041		4.8×10^{-4}		
		0.0095		7.8×10^{-4}		
		0.015		11×10^{-4}		
					6.0×10^{-2}	2.1×10^{-4}
		0.0014	1600	2.7×10^{-4}		
		0.0041		4.8×10^{-4}		
		0.012		10×10^{-4}		
		0.015		12×10^{-4}		
					6.8×10^{-2}	1.9×10^{-4}

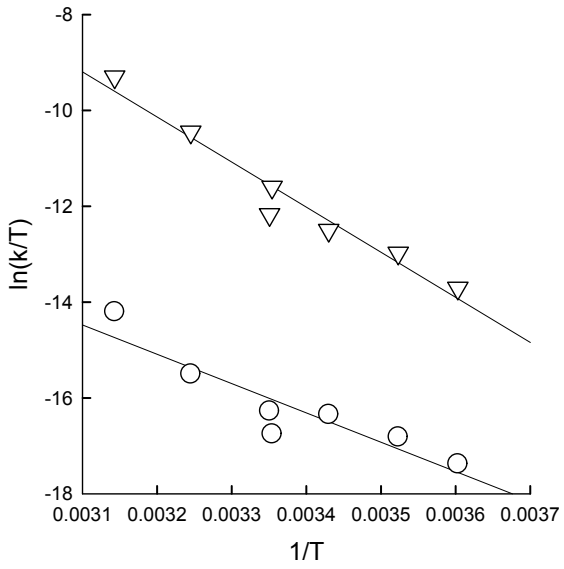

Figure S1.- Eyring plot for the temperature dependence of the k_+ (▽) and k_- (○) rate constants for the reaction of cluster [**1**]$^+$ with PhA.

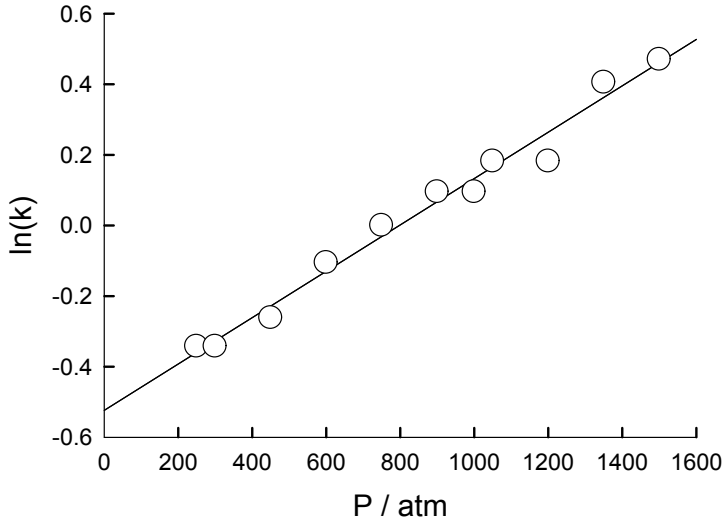

Figure S2.- ln(k) *versus* P plot for the k_+ rate constant for the reaction of cluster [**1**]$^+$ with dmad.

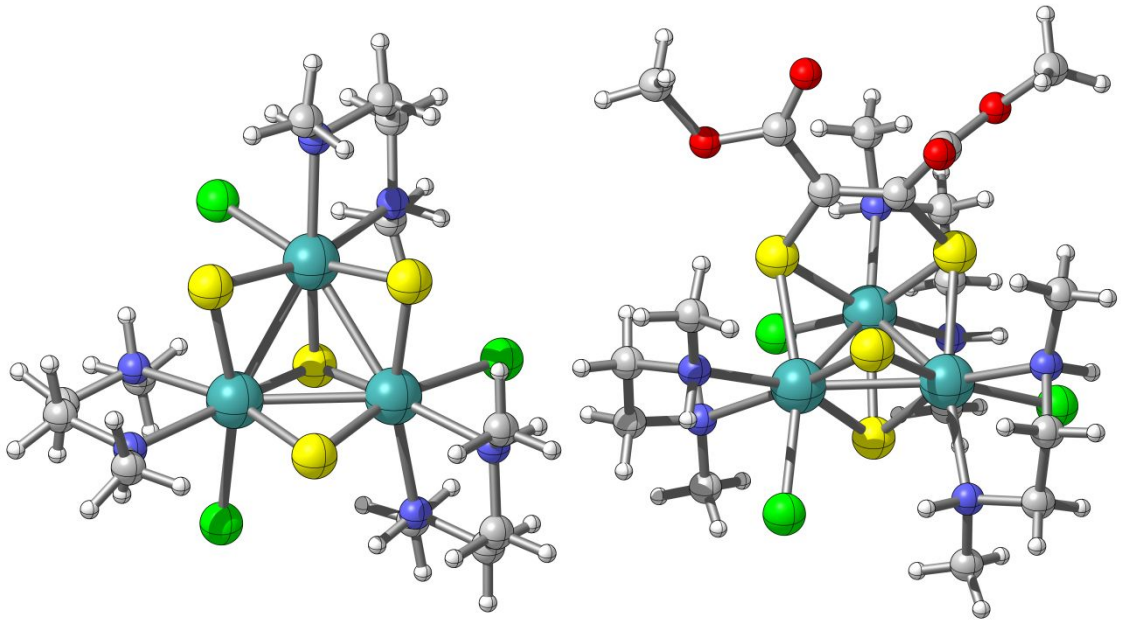

Figure S3.- Structure of [**1**]$^{+}$ (left) and [**1-dmad**]$^{+}$ (right). Colour code: Mo(cyan); S (yellow); N (blue); O (red); C (grey); H (white).

Table S3. For [**1**]$^{+}$, summary of selected average bond lengths (Å) computed for each DFT functional in the gas phase using the BS1 basis set system, and its mean unsigned error (MUE) with respect to the X-ray structure.

	Mo-Mo	Mo-(μ_3-S)	Mo-(μ-S)[b]	Mo-(μ-S)[c]	Mo-N[d]	Mo-N[e]	Mo-Cl	MUE
X-ray[a]	2.759	2.335	2.301	2.288	2.278	2.298	2.492	[g]
BP86	2.793	2.375	2.335	2.326	2.316	2.347	2.503	0.035
B3LYP	2.796	2.372	2.328	2.317	2.326	2.356	2.516	0.037
PBE0[f]	2.754	2.349	2.309	2.297	2.287	2.315	2.484	0.01
TPSS	2.776	2.377	2.337	2.326	2.304	2.328	2.494	0.027
TPSSh	2.764	2.367	2.327	2.315	2.295	2.319	2.489	0.019
M06HF	2.691	2.318	2.292	2.271	2.256	2.281	2.507	0.024
M06	2.779	2.364	2.321	2.315	2.305	2.334	2.496	0.023
M062X	2.724	2.339	2.306	2.292	2.306	2.332	2.522	0.02
M06L	2.749	2.362	2.325	2.318	2.326	2.35	2.507	0.029
M11	2.735	2.343	2.308	2.293	2.293	2.318	2.511	0.014
wB97XD	2.754	2.349	2.31	2.301	2.301	2.328	2.502	0.015
B97D3	2.773	2.361	2.323	2.317	2.307	2.335	2.506	0.025
BP86D3(BJ)	2.765	2.365	2.328	2.321	2.287	2.315	2.49	0.018
B3LYPD3(BJ)	2.768	2.362	2.322	2.311	2.296	2.322	2.502	0.019
PBE0D3(BJ)	2.741	2.344	2.306	2.295	2.273	2.3	2.478	0.009
PBE0D3(0)	2.745	2.346	2.309	2.298	2.283	2.31	2.483	0.01

[a] Obtained from: E. Pedrajas, I. Sorribes, K. Junge, M. Beller, R. Llusar, *ChemCatChem* **2015**, *7*, 2675-2681; [b] Mo–(μ-S) length *trans* to the Mo–N bond; [c] Mo–(μ-S) length *trans* to the Mo–Cl bond; [d] Mo–N length *trans* to the Mo–(μ_3-S) bond; [e] Mo–N length *cis* to the Mo–(μ_3-S) bond; [f] Optimizations including the effects of the solvent self-consistently via

PCM and SMD approaches led to MUE values of 0.009 and 0.010, respectively. [g] The average uncertainty on the selected XRD-determined distances is 0.008 Å.

Table S4. For [**1-dmad**]$^{+}$,[a] summary of average selected bond lengths (Å) computed for each DFT functional in the gas phase using the BS1 basis set system, and its mean unsigned error (MUE) with respect to the X-ray structure.

	Mo(1)-Mo(2)	Mo(3)-Mo(1&2)	Mo(3)-(μ-S)	S-C	C=C	Mo(3)-(μ_3-S)	Mo(3)-Cl	MUE
X-Ray[b]	2.653	2.775	2.355	1.812	1.33	2.321	2.485	[d]
BP86	2.673	2.798	2.384	1.854	1.349	2.356	2.507	0.027
B3LYP	2.672	2.802	2.389	1.835	1.339	2.343	2.526	0.025
PBE0[c]	2.639	2.757	2.363	1.819	1.336	2.325	2.491	0.009
TPSS	2.659	2.777	2.389	1.852	1.346	2.358	2.498	0.021
TPSSh	2.648	2.764	2.382	1.838	1.341	2.346	2.494	0.017
M06HF	2.638	2.784	2.36	1.805	1.33	2.289	2.511	0.013
M06	2.662	2.788	2.385	1.823	1.335	2.34	2.503	0.01

								5
M062X	2.63	2.749	2.374	1.813	1.334	2.315	2.54	0.019
M06L	2.636	2.753	2.388	1.827	1.339	2.346	2.511	0.021
M11	2.651	2.791	2.379	1.81	1.336	2.307	2.534	0.016
wB97XD	2.642	2.763	2.366	1.82	1.332	2.324	2.518	0.011
B97D3	2.653	2.776	2.372	1.842	1.345	2.344	2.503	0.015
BP86D3(BJ)	2.65	2.769	2.379	1.826	1.337	2.339	2.507	0.013
B3LYPD3(BJ)	2.65	2.769	2.379	1.825	1.337	2.339	2.507	0.013
PBE0D3(BJ)	2.628	2.742	2.358	1.815	1.335	2.323	2.482	0.011
PBE0D3(0)	2.632	2.747	2.361	1.818	1.336	2.324	2.486	0.01

[a] Note that the three Mo centres in this structure are not equivalent (see Scheme 1). Herein the one involved in the [3+2] cycloaddition process has been labelled as Mo(3); [b] Obtained from: A. G. Algarra, E. Guillamón, J. Andrés, M. J. Fernández-Trujillo, E. Pedrajas, J. Á. Pino-Chamorro, R. Llusar, M. G. Basallote, *ACS Catal.*, **2018**, *8*, 7346-7350; [c] Optimizations including the effects of the solvent self-consistently via PCM and SMD approaches led to a MUE value of 0.011 in both cases. [d] The average uncertainty on the selected XRD-determined distances is 0.003 Å.

Table S5. Computed activation free energies ($\Delta G^{\ddagger}$, kcal/mol) for the forward and reverse reactions of [**1**]$^{+}$ with phenylacetylene (R1 and R2, respectively) and the forward reaction of [**1**]$^{+}$ with dmad (R3), and its mean unsigned error (MUE) with respect to the experimental values.

Entry	Level of theory	Solvent = PCM				Solvent = SMD			
		R1	R2	R3	*MUE*	R1	R2	R3	MUE
1	*Experimental*	*20.8*	*23.3*	*17.7*		*20.8*	*23.3*	*17.7*	
2	BP86(BS2,Solvent)/BP86(BS1)	26.1	13.8	24.6	*7.2*	28.1	13.8	26.5	*8.5*
3	BP86D3(0)(BS2,Solvent)/BP86(BS1)	9.7	12.8	7.1	*10.7*	11.7	12.9	9.0	*9.4*
4	BP86D3(BJ)(BS2,Solvent)/BP86(BS1)	5.9	15.8	3.9	*12.1*	7.9	15.8	5.9	*10.7*
5	TPSS(BS2,Solvent)/TPSS(BS1)	26.8	13.8	24.4	*7.4*	28.8	13.8	26.2	*8.7*
6	TPSSD3(0)(BS2,Solvent)/TPSS(BS1)	14.1	13.2	10.7	*7.9*	16.1	13.2	12.5	*6.7*
7	TPSSD3(BJ)(BS2,Solvent)/TPSS(BS1)	11.4	15.1	8.4	*9.0*	13.4	15.1	10.2	*7.7*
8	TPSSh(BS2,Solvent)/TPSSh(BS1)	28.3	16.4	25.8	*7.5*	30.3	16.4	27.6	*8.8*
9	TPSShD3(0)(BS2,Solvent)/TPSSh(BS1)	15.7	15.9	12.1	*6.0*	17.6	15.9	13.9	*4.8*

10	TPSShD3(BJ)(BS2,Solvent)/TPSSh(BS1)	12.9	17.7	9.5	*7.2*	14.8	17.7	11.4	*6.0*
11	B3LYP(BS2,Solvent)/B3LYP(BS1)	36.1	16.4	32.8	*12.4*	38.0	16.3	34.9	*13.8*
12	B3LYPD3(0)(BS2,Solvent)/B3LYP(BS1)	21.8	15.8	17.2	*3.0*	23.7	15.6	19.3	*4.0*
13	B3LYPD3(BJ)(BS2,Solvent)/B3LYP(BS1)	17.9	18.4	13.4	*4.0*	19.8	18.3	15.5	*2.7*
14	PBE0(BS2,Solvent)/PBE0(BS1)	27.7	22.1	24.7	*5.1*	29.7	22.0	26.5	*6.3*
15	PBE0D3(0)(BS2,Solvent)/PBE0(BS1)	17.5	21.7	13.6	*3.0*	19.4	21.6	15.3	*1.8*
16	PBE0D3(BJ)(BS2,Solvent)/PBE0(BS1)	15.7	23.1	12.0	*3.7*	17.6	23.0	13.8	*2.5*
17	M06L(BS2,Solvent)/M06L(BS1)	19.8	13.7	17.6	*3.6*	21.8	13.8	18.9	*3.9*
18	M06LD3(0)(BS2,Solvent)/M06L(BS1)	17.6	13.7	15.1	*5.1*	19.6	13.8	16.5	*3.9*
19	M06(BS2,Solvent)/M06(BS1)	24.4	18.0	a	*4.4*	26.4	18.1	a	*5.4*
20	M06D3(0)(BS2,Solvent)/M06(BS1)	20.2	18.1	a	*2.9*	22.3	18.1	a	*3.3*
21	M06-2X(BS2,Solvent)/M06-2X(BS1)	25.6	23.3	20.8	*2.6*	27.6	23.1	22.5	*3.9*
22	M06-2XD3(0)(BS2,Solvent)/M06-2X(BS1)	23.7	23.3	18.6	*1.3*	25.7	23.1	20.3	*2.5*
23	M06-HF(BS2,Solvent)/M06-HF(BS1)	20.9	36.4	16.7	*4.7*	22.9	36.2	18.6	*5.3*

24	M06-HFD3(0)(BS2,Solvent)/M06-HF(BS1)	17.9	36.5	13.3	*6.9*	19.9	36.3	15.2	*5.4*
25	B97D3(BS2,Solvent)/B97D3(BS1)	12.2	12.7	9.6	*9.1*	14.2	12.8	11.1	*7.9*
26	M11(BS2,Solvent)/M11(BS1)	26.5	29.1	20.9	*4.9*	28.5	28.9	22.5	*6.0*
27	wB97XD(BS2,Solvent)/wB97XD(BS1)	12.1	10.7	8.1	*10.3*	26.8	22.8	22.7	*3.8*
28	BP86D3(BJ)(BS2,Solvent)/BP86D3(BJ)(BS1)	5.5	15.8	17.1	*7.8*	7.6	15.8	18.7	*7.2*
29	B3LYPD3(BJ)(BS2,Solvent)/B3LYPD3(BJ)(BS1)	17.2	18.1	12.5	*4.7*	19.3	18.1	14.1	*3.4*
30	PBE0D3(BJ)(BS2,Solvent)/PBE0D3(BJ)(BS1)	15.8	23.0	12.0	*3.7*	17.9	23.0	13.6	*2.5*
31	PBE0D3(0)(BS2,Solvent)/PBE0D3(0)(BS1)	17.8	21.8	13.6	*2.9*	19.9	21.8	15.3	*1.6*

[a] Despite multiple attempts, the transition state for the process at this level of theory could not be optimized.

Table S6. Computed activation volumes ($\Delta V^{\ddagger}$, cm^3mol^{-1}) for the forward and reverse reactions of $[\mathbf{1}]^+$ with phenylacetylene (R1 and R2, respectively) and the forward reaction of $[\mathbf{1}]^+$ with dmad (R3), and its mean unsigned error (MUE) with respect to the experimental values.

Entry	Level of theory	radii = scaled UFF				radii = unscaled SMD-Coulomb			
		R1	R2	R3	*MUE*	R1	R2	R3	MUE
	Experimental	*-14*	*4*	*-16*		*-14*	*4*	*-16*	
41	BP86(BS2,Solvent)/BP86(BS1)	-18.6	4.8	-20.3	3.2	-12.3	3.8	-17.8	1.2
42	TPSS(BS2,Solvent)/TPSS(BS1)	-18.8	4.6	-20.3	3.2	-11.9	4.4	-18.1	1.6
43	TPSSh(BS2,Solvent)/TPSSh(BS1)	-19.7	4.0	-21.0	3.6	-12.3	4.1	-18.7	1.5
44	B3LYP(BS2,Solvent)/B3LYP(BS1)	-17.5	4.7	-19.2	2.5	-11.9	3.7	-18.4	1.6
45	PBE0(BS2,Solvent)/PBE0(BS1)	-18.6	4.1	-19.8	2.8	-12.4	3.5	-19.1	1.7
46	M06L(BS2,Solvent)/M06L(BS1)	-20.4	3.6	-21.5	4.1	-13.4	3.4	-21.5	2.2
47	M06(BS2,Solvent)/M06(BS1)	-21.3	3.0	[b]	4.1	-13.6	2.9	[b]	0.7
48	M06-2X(BS2,Solvent)/M06-2X(BS1)	-18.6	3.4	-21.3	3.5	-13.3	3.0	-21.9	2.5
49	M06-HF(BS2,Solvent)/M06-HF(BS1)	-18.7	2.4	-21.4	3.9	-13.7	1.1	-20.7	2.6
50	M11(BS2,Solvent)/M11(BS1)	-19.6	2.3	-22.1	4.4	-13.3	1.9	-22.0	2.9
51	B97D3(BS2,Solvent)/B97D3(BS1)	-19.2	4.4	-19.7	3.1	-12.2	4.5	-19.3	1.8

52	wB97XD(BS2,Solvent)/wB97XD(BS1)	-19.2	4.3	-20.6	3.3	-12.5	4.4	-20.9	2.3
53	BP86D3(BJ)(BS2,Solvent)/BP86D3(BJ)(BS1)	-18.8	5.7	-22.1	4.2	-13.7	3.9	-21.3	1.9
54	B3LYPD3(BJ)(BS2,Solvent)/B3LYPD3(BJ)(BS1)	-21.7	3.3	-22.3	4.9	-13.4	3.8	-20.7	1.8
55	PBE0D3(BJ)(BS2,Solvent)/PBE0D3(BJ)(BS1)	-19.3	4.5	-20.3	3.4	-12.9	4.1	-19.8	1.7
56	PBE0D3(0)(BS2,Solvent)/PBE0D3(0)(BS1)	-20.0	4.0	-20.9	3.6	-13.4	3.7	-20.1	1.7

[b] Despite multiple attempts, the transition state for the process at this level of theory could not be optimized.

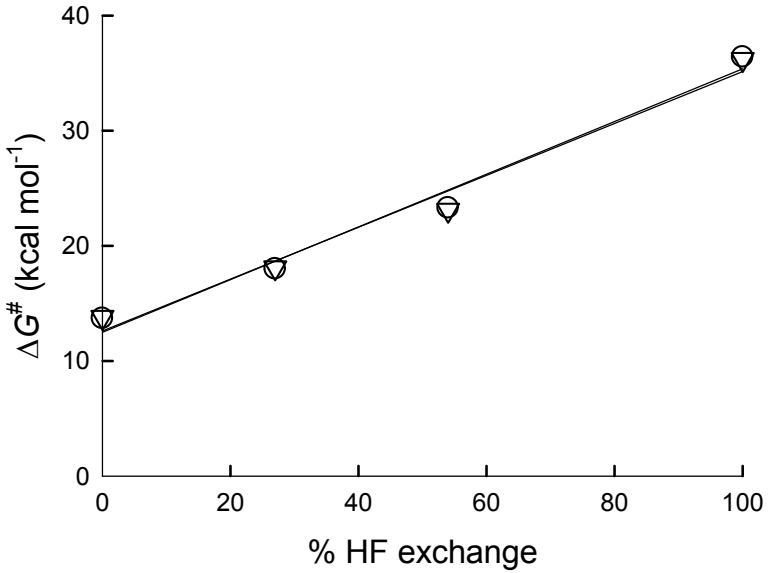

Figure S4.- Computed $\Delta G^{\#}$ values at the Functional(BS2,Solvent)/Functional(BS1) (Functional = M06-L, M06, M06-2X, M06-HF; Solvent= PCM (○); SMD (▽)) level of theory for the reverse reaction between [**1**]$^{+}$ and PhA (labelled as R2) as a function of the % of Hartree-Fock exchange of the M06 functional (for M06L, %HF = 0%; for M06, %HF = 27%; for M06-2X, %HF = 54%; for M06HF, %HF = 100%).

Table S7. Computed energies (Hartrees) and vdW volumes (cm^3mol^{-1}) for the optimized structures associated with the study of $[\mathbf{1}]^+$.

BP86/BS1 optimized structures	$[\mathbf{1}]^+$	PhA	TS ($[\mathbf{1}]^+$,PhA)	Prod ($[\mathbf{1}]^+$,PhA)	DMAD	TS ($[\mathbf{1}]^+$,DMAD)	Prod ($[\mathbf{1}]^+$,DMAD)
E(BS1)	-2434.44018	-308.38426	-2742.81108	-2742.83938	-533.08076	-2967.51742	-2967.54069
Thermal corr. to H (298 K)	0.55876	0.11377	0.67286	0.67532	0.12336	0.68255	0.68408
Thermal corr. to G (298 K)	0.45281	0.07549	0.54901	0.55427	0.07182	0.54702	0.55128
D3(0) corr.	-0.15784	-0.00820	-0.19215	-0.19066	-0.01027	-0.19592	-0.19751
D3(BJ) corr.	-0.25464	-0.02237	-0.30924	-0.31247	-0.01839	-0.30589	-0.31302
Standard State Corr.	0.00302	0.00302	0.00302	0.00302	0.00302	0.00302	0.00302
Symmetry Corr.	0.00104	0.00065	0.00000	0.00000	0.00065	0.00000	0.00000
E(BS2,PCM)	-2434.82164	-308.47814	-2743.27417	-2743.30139	-533.26950	-2968.06968	-2968.09262
E(BS2,SMD)	-2434.85140	-308.48425	-2743.30684	-2743.33407	-533.27241	-2968.09928	-2968.12192
Volume (PCM)	691.986	171.167	832.185	824.157	201.854	860.197	850.071
Volume (SMD)	610.423	120.845	710.87	704.527	189.981	770.873	755.482
TPSS/BS1 optimized structures	$[\mathbf{1}]^+$	PhA	TS ($[\mathbf{1}]^+$,PhA)	Prod ($[\mathbf{1}]^+$,PhA)	DMAD	TS ($[\mathbf{1}]^+$,DMAD)	Prod ($[\mathbf{1}]^+$,DMAD)
E(BS1)	-2434.16293	-308.45476	-2742.60334	-2742.63122	-533.15862	-2967.31784	-2967.34048
Thermal corr. to H (298 K)	0.56755	0.11534	0.68320	0.68570	0.12516	0.69307	0.69463
Thermal corr. to G (298 K)	0.46275	0.07723	0.56096	0.56589	0.07385	0.55902	0.56300
D3(0) corr.	-0.11349	-0.00599	-0.13980	-0.13893	-0.00728	-0.14261	-0.14378
D3(BJ) corr.	-0.18639	-0.01785	-0.22880	-0.23096	-0.01502	-0.22691	-0.23152
Standard State Corr.	0.00302	0.00302	0.00302	0.00302	0.00302	0.00302	0.00302
Symmetry Corr.	0.00104	0.00065	0.00000	0.00000	0.00065	0.00000	0.00000
E(BS2,PCM)	-2434.52908	-308.54310	-2743.04569	-2743.07256	-533.34083	-2967.84874	-2967.87081
E(BS2,SMD)	-2434.55797	-308.54906	-2743.07737	-2743.10426	-533.34355	-2967.87745	-2967.89911
Volume (PCM)	687.166	170.607	826.517	818.94	201.309	854.778	844.74
Volume (SMD)	606.971	120.559	707.817	700.446	189.484	766.404	751.514
TPSSh/BS1 optimized structures	$[\mathbf{1}]^+$	PhA	TS ($[\mathbf{1}]^+$,PhA)	Prod ($[\mathbf{1}]^+$,PhA)	DMAD	TS ($[\mathbf{1}]^+$,DMAD)	Prod ($[\mathbf{1}]^+$,DMAD)
E(BS1)	-2434.01234	-308.42203	-2742.41670	-2742.44963	-533.09353	-2967.09931	-2967.12668
Thermal corr. to H (298 K)	0.57399	0.11672	0.69096	0.69365	0.12685	0.70123	0.70292
Thermal corr. to G (298 K)	0.47047	0.07879	0.57019	0.57541	0.07589	0.56915	0.57306
D3(0) corr.	-0.11374	-0.00581	-0.13973	-0.13894	-0.00714	-0.14272	-0.14370
D3(BJ) corr.	-0.17930	-0.01648	-0.22045	-0.22249	-0.01380	-0.21903	-0.22315
Standard State Corr.	0.00302	0.00302	0.00302	0.00302	0.00302	0.00302	0.00302
Symmetry Corr.	0.00104	0.00065	0.00000	0.00000	0.00065	0.00000	0.00000
E(BS2,PCM)	-2434.37233	-308.50813	-2742.85152	-2742.88289	-533.27189	-2967.62116	-2967.64773
E(BS2,SMD)	-2434.40114	-308.51423	-2742.88329	-2742.91461	-533.27460	-2967.64980	-2967.67586
Volume (PCM)	683.536	170.084	820.831	814.226	200.633	849.375	839.735
Volume (SMD)	603.249	120.26	703.087	696.338	188.891	761.123	746.952
B3LYP/BS1 optimized structures	$[\mathbf{1}]^+$	PhA	TS ($[\mathbf{1}]^+$,PhA)	Prod ($[\mathbf{1}]^+$,PhA)	DMAD	TS ($[\mathbf{1}]^+$,DMAD)	Prod ($[\mathbf{1}]^+$,DMAD)
E(BS1)	-2433.96572	-308.39660	-2742.33477	-2742.36763	-533.07364	-2967.02552	-2967.05169
Thermal corr. to H (298 K)	0.57462	0.11690	0.69182	0.69465	0.12705	0.70210	0.70388
Thermal corr. to G (298 K)	0.47011	0.07909	0.57058	0.57536	0.07635	0.56990	0.57281
D3(0) corr.	-0.14139	-0.00709	-0.17128	-0.17028	-0.00896	-0.17527	-0.17633

D3(BJ) corr.	-0.24920	-0.02451	-0.30272	-0.30599	-0.02043	-0.30057	-0.30606
Standard State Corr.	0.00302	0.00302	0.00302	0.00302	0.00302	0.00302	0.00302
Symmetry Corr.	0.00104	0.00065	0.00000	0.00000	0.00065	0.00000	0.00000
E(BS2,PCM)	-2434.34756	-308.49253	-2742.79922	-2742.83013	-533.26444	-2967.57843	-2967.60294
E(BS2,SMD)	-2434.37789	-308.49861	-2742.83263	-2742.86331	-533.26731	-2967.60833	-2967.63275
Volume (PCM)	690.593	169.96	831.557	823.67	200.589	859.358	850.051
Volume (SMD)	610.014	120.183	710.378	704.224	189.11	768.506	756.234
M06L/BS1 optimized structures	[**1**]$^+$	PhA	TS ([**1**]$^+$,PhA)	Prod ([**1**]$^+$,PhA)	DMAD	TS ([**1**]$^+$,DMAD)	Prod ([**1**]$^+$,DMAD)
E(BS1)	-2433.92230	-308.35688	-2742.27443	-2742.30222	-533.02438	-2966.95081	-2966.97467
Thermal corr. to H (298 K)	0.57281	0.11692	0.68977	0.69262	0.12690	0.69991	0.70172
Thermal corr. to G (298 K)	0.47005	0.07908	0.57130	0.57565	0.07618	0.57046	0.57339
D3(0) corr.	-0.00808	-0.00030	-0.01179	-0.01181	-0.00038	-0.01232	-0.01250
Standard State Corr.	0.00302	0.00302	0.00302	0.00302	0.00302	0.00302	0.00302
Symmetry Corr.	0.00104	0.00065	0.00000	0.00000	0.00065	0.00000	0.00000
E(BS2,PCM)	-2434.27542	-308.43609	-2742.69745	-2742.72359	-533.18752	-2967.45446	-2967.47654
E(BS2,SMD)	-2434.30332	-308.44158	-2742.72766	-2742.75403	-533.18980	-2967.48250	-2967.50364
Volume (PCM)	682.635	169.639	818.373	812.441	199.838	846.726	838.649
Volume (SMD)	603.379	119.969	701.085	695.458	188.083	755.692	746.768
M06/BS1 optimized structures	[**1**]$^+$	PhA	TS ([**1**]$^+$,PhA)	Prod ([**1**]$^+$,PhA)			
E(BS1)	-2433.10343	-308.14467	-2741.23843	-2741.27305			
Thermal corr. to H (298 K)	0.57010	0.11663	0.68663	0.68929			
Thermal corr. to G (298 K)	0.46719	0.07880	0.56814	0.57177			
D3(0) corr.	-0.01925	-0.00106	-0.02699	-0.02709			
Standard State Corr.	0.00302	0.00302	0.00302	0.00302			
Symmetry Corr.	0.00104	0.00065	0.00000	0.00000			
E(BS2,PCM)	-2433.46828	-308.23525	-2741.68209	-2741.71446			
E(BS2,SMD)	-2433.49761	-308.24122	-2741.71414	-2741.74655			
Volume (PCM)	685.675	169.592	819.965	814.994			
Volume (SMD)	604.057	119.913	701.411	696.531			
M062X/BS1 optimized structures	[**1**]$^+$	PhA	TS ([**1**]$^+$,PhA)	Prod ([**1**]$^+$,PhA)	DMAD	TS ([**1**]$^+$,DMAD)	Prod ([**1**]$^+$,DMAD)
E(BS1)	-2432.93926	-308.25921	-2741.18618	-2741.22990	-532.85937	-2965.80087	-2965.84134
Thermal corr. to H (298 K)	0.57899	0.11817	0.69733		0.12905	0.70837	0.71039
Thermal corr. to G (298 K)	0.47755	0.08050	0.58080		0.07881	0.58117	0.58327
D3(0) corr.	-0.00716	-0.00025	-0.01045	-0.01051	-0.00033	-0.01103	-0.01116
Standard State Corr.	0.00302	0.00302	0.00302	0.00302	0.00302	0.00302	0.00302
Symmetry Corr.	0.00104	0.00065	0.00000	0.00000	0.00065	0.00000	0.00000
E(BS2,PCM)	-2433.35267	-308.35598	-2741.68584	-2741.72659	-533.04927	-2966.38894	-2966.42584
E(BS2,SMD)	-2433.38225	-308.36254	-2741.71891	-2741.75939	-533.05218	-2966.41871	-2966.45534
Volume (PCM)	677.9	169.593	816.541	810.953	199.861	842.4	837.832
Volume (SMD)	600.507	119.95	698.325	693.373	188.266	752.426	745.726
M06HF/BS1 optimized structures	[**1**]$^+$	PhA	TS ([**1**]$^+$,PhA)	Prod ([**1**]$^+$,PhA)	DMAD	TS ([**1**]$^+$,DMAD)	Prod ([**1**]$^+$,DMAD)
E(BS1)	-2432.81097	-308.31344	-2741.11789	-2741.18254	-532.88123	-2965.70186	-2965.76681
Thermal corr. to H (298 K)	0.58802	0.11961	0.70788	0.71028	0.13144	0.72028	0.72177
Thermal corr. to G (298 K)	0.48788	0.08207	0.59330	0.59555	0.08054	0.59522	0.59730
D3(0) corr.	-0.01297	-0.00056	-0.01831	-0.01847	-0.00063	-0.01902	-0.01931

Standard State Corr.	0.00302	0.00302	0.00302	0.00302	0.00302	0.00302	0.00302
Symmetry Corr.	0.00104	0.00065	0.00000	0.00000	0.00065	0.00000	0.00000
E(BS2,PCM)	-2433.33401	-308.42543	-2741.74482	-2741.80508	-533.10482	-2966.43435	-2966.49529
E(BS2,SMD)	-2433.36391	-308.43313	-2741.77916	-2741.83904	-533.10814	-2966.46452	-2966.52520
Volume (PCM)	669.633	169.432	808.006	804.065	199.609	833.689	829.706
Volume (SMD)	591.747	119.884	688.924	687.084	188.067	745.465	737.724
M11/BS1 optimized structures	[**1**]$^+$	PhA	TS ([**1**]$^+$,PhA)	Prod ([**1**]$^+$,PhA)	DMAD	TS ([**1**]$^+$,DMAD)	Prod ([**1**]$^+$,DMAD)
E(BS1)	-2432.82260	-308.18208	-2740.98946	-2741.04254	-532.81101	-2965.63573	-2965.68532
Thermal corr. to H (298 K)	0.57511	0.11745	0.69285	0.69559	0.12797	0.70363	0.70559
Thermal corr. to G (298 K)	0.47441	0.07980	0.57734	0.58050	0.07772	0.57737	0.58014
Standard State Corr.	0.00302	0.00302	0.00302	0.00302	0.00302	0.00302	0.00302
Symmetry Corr.	0.00104	0.00065	0.00000	0.00000	0.00065	0.00000	0.00000
E(BS2,PCM)	-2433.26634	-308.28796	-2741.53046	-2741.58008	-533.01809	-2966.27173	-2966.31794
E(BS2,SMD)	-2433.29573	-308.29485	-2741.56364	-2741.61290	-533.02104	-2966.30136	-2966.34678
Volume (PCM)	678.012	169.924	815.396	811.544	200.253	841.642	837.538
Volume (SMD)	599.327	120.087	697.331	694.245	188.38	751.204	744.486
B97D3/BS1 optimized structures	[**1**]$^+$	PhA	TS ([**1**]$^+$,PhA)	Prod ([**1**]$^+$,PhA)	DMAD	TS ([**1**]$^+$,DMAD)	Prod ([**1**]$^+$,DMAD)
E(BS1)	-2434.20215	-308.18620	-2742.39912	-2742.42559	-532.75484	-2966.97897	-2967.00183
Thermal corr. to H (298 K)	0.56593	0.11462	0.68138	0.68400	0.12437	0.69109	0.69300
Thermal corr. to G (298 K)	0.46153	0.07641	0.56103	0.56558	0.07273	0.55880	0.56332
Standard State Corr.	0.00302	0.00302	0.00302	0.00302	0.00302	0.00302	0.00302
Symmetry Corr.	0.00104	0.00065	0.00000	0.00000	0.00065	0.00000	0.00000
E(BS2,PCM)	-2434.57569	-308.27650	-2742.85061	-2742.87542	-532.94081	-2967.52041	-2967.54272
E(BS2,SMD)	-2434.60496	-308.28241	-2742.88251	-2742.90752	-532.94359	-2967.55011	-2967.57164
Volume (PCM)	684.229	170.656	822.899	815.555	201.466	852.989	842.417
Volume (SMD)	604.635	120.57	704.853	697.418	189.78	762.398	750.486
wB97XD/BS1 optimized structures	[**1**]$^+$	PhA	TS ([**1**]$^+$,PhA)	Prod ([**1**]$^+$,PhA)	DMAD	TS ([**1**]$^+$,DMAD)	Prod ([**1**]$^+$,DMAD)
E(BS1)	-2433.72104	-308.28300	-2741.99155	-2742.03637	-532.89790	-2966.62128	-2966.65992
Thermal corr. to H (298 K)	0.58131	0.11822	0.69958	0.70254	0.12860	0.71056	0.71230
Thermal corr. to G (298 K)	0.48033	0.08057	0.58227	0.58716	0.07817	0.58366	0.58591
Standard State Corr.	0.00302	0.00302	0.00302	0.00302	0.00302	0.00302	0.00302
Symmetry Corr.	0.00104	0.00065	0.00000	0.00000	0.00065	0.00000	0.00000
E(BS2,PCM)	-2434.08377	-308.36963	-2742.45080	-2742.47269	-533.07463	-2967.16587	-2967.20173
E(BS2,SMD)	-2434.13362	-308.37597	-2742.48358	-2742.52474	-533.07745	-2967.19538	-2967.23055
Volume (PCM)	680.304	169.593	818.076	810.991	199.982	846.076	836.835
Volume (SMD)	601.283	119.953	700.487	693.215	188.513	755.115	744.55
BP86-D3(BJ)/BS1 optimized structures	[**1**]$^+$	PhA	TS ([**1**]$^+$,PhA)	Prod ([**1**]$^+$,PhA)	DMAD	TS ([**1**]$^+$,DMAD)	Prod ([**1**]$^+$,DMAD)
E(BS1)	-2434.69740	-308.40663	-2743.12556	-2743.15623	-533.09916	-2967.33043	-2967.36176
Thermal corr. to H (298 K)	0.55996	0.11385	0.67446	0.67684	0.12342	0.70390	0.00378
Thermal corr. to G (298 K)	0.45619	0.07554	0.55454	0.55859	0.07173	0.57428	-0.25733
Standard State Corr.	0.00302	0.00302	0.00302	0.00302	0.00302	0.00302	0.00302
Symmetry Corr.	0.00104	0.00065	0.00000	0.00000	0.00065	0.00000	0.00000
E(BS2,PCM)	-2435.07933	-308.50057	-2743.58926	-2743.61846	-533.28791	-2968.38161	-2968.40837
E(BS2,SMD)	-2435.10856	-308.50667	-2743.62119	-2743.65046	-533.29081	-2968.41122	-2968.43733
Volume (PCM)	681.626	171.05	821.383	811.975	201.716	846.574	837.538

Volume (SMD)	602.501	120.767	700.554	694.041	189.84	757.01	745.559
B3LYP-D3(BJ) /BS1 optimized structures	[**1**]$^+$	PhA	TS ([**1**]$^+$,PhA)	Prod ([**1**]$^+$,PhA)	DMAD	TS ([**1**]$^+$,DMAD)	Prod ([**1**]$^+$,DMAD)
E(BS1)	-2434.21765	-308.42112	-2742.64218	-2742.67800	-533.09407	-2967.33040	-2967.36174
Thermal corr. to H (298 K)	0.57608	0.11699	0.69366	0.69647	0.12712	0.70385	0.00378
Thermal corr. to G (298 K)	0.47376	0.07917	0.57514	0.58000	0.07621	0.57421	-0.25733
Standard State Corr.	0.00302	0.00302	0.00302	0.00302	0.00302	0.00302	0.00302
Symmetry Corr.	0.00104	0.00065	0.00000	0.00000	0.00065	0.00000	0.00000
E(BS2,PCM)	-2434.59949	-308.51711	-2743.10663	-2743.14030	-533.28488	-2967.88396	-2967.91349
E(BS2,SMD)	-2434.62911	-308.52319	-2743.13911	-2743.17289	-533.28774	-2967.91385	-2967.94270
Volume (PCM)	683.172	169.851	816.944	811.422	200.468	846.607	837.602
Volume (SMD)	602.41	120.112	700.226	693.897	188.97	757.033	745.493
PBE0-D3(BJ) /BS1 optimized structures	[**1**]$^+$	PhA	TS ([**1**]$^+$,PhA)	Prod ([**1**]$^+$,PhA)	DMAD	TS ([**1**]$^+$,DMAD)	Prod ([**1**]$^+$,DMAD)
E(BS1)	-2432.60735	-308.03435	-2740.64568	-2740.68878	-532.49505	-2965.11856	-2965.15848
Thermal corr. to H (298 K)	0.57873	0.11782	0.69698	0.69979	0.12824	0.70755	0.70947
Thermal corr. to G (298 K)	0.47759	0.08006	0.58004	0.58454	0.07758	0.57886	0.58316
Standard State Corr.	0.00302	0.00302	0.00302	0.00302	0.00302	0.00302	0.00302
Symmetry Corr.	0.00104	0.00065	0.00000	0.00000	0.00065	0.00000	0.00000
E(BS2,PCM)	-2432.96026	-308.11860	-2741.07137	-2741.11250	-532.66900	-2965.62909	-2965.66807
E(BS2,SMD)	-2432.98936	-308.12507	-2741.10364	-2741.14480	-532.67190	-2965.65862	-2965.69678
Volume (PCM)	673.125	169.579	810.595	803.187	199.784	839.201	828.883
Volume (SMD)	594.863	119.93	693.298	686.483	188.09	750.017	736.44
PBE0D3(0)/BS1 optimized structures	[**1**]$^+$	PhA	TS ([**1**]$^+$,PhA)	Prod ([**1**]$^+$,PhA)	DMAD	TS ([**1**]$^+$,DMAD)	Prod ([**1**]$^+$,DMAD)
E(BS1)	-2432.55887	-308.02636	-2740.58616	-2740.62725	-532.49002	-2965.06263	-2965.10013
Thermal corr. to H (298 K)	0.57903	0.11779	0.69722	0.70004	0.12817	0.70776	0.70964
Thermal corr. to G (298 K)	0.47864	0.08002	0.58114	0.58556	0.07767	0.58023	0.58415
Standard State Corr.	0.00302	0.00302	0.00302	0.00302	0.00302	0.00302	0.00302
Symmetry Corr.	0.00104	0.00065	0.00000	0.00000	0.00065	0.00000	0.00000
E(BS2,PCM)	-2432.91154	-308.11058	-2741.01161	-2741.05076	-532.66395	-2965.57307	-2965.60927
E(BS2,SMD)	-2432.94100	-308.11706	-2741.04406	-2741.08316	-532.66652	-2965.60237	-2965.63757
E(BS1,PCM)	-2432.62055	-308.03094	-2740.64720	-2740.68817	-532.49857	-2965.12678	-2965.16414
E(BS1,SMD)	-2432.64957	-308.03742	-2740.67896	-2740.72007	-532.50064	-2965.15554	-2965.19206
E(BS4,PCM)	-3983.59680	-308.04950	-4291.63812	-4291.68079	-532.53438	-4286.82539	-4286.72589
E(BS4,SMD)	-3983.62483	-308.05561	-4291.66876	-4291.71145	-532.53629	-4516.16473	-4516.20407
E(BS5,PCM)	-3984.50072	-308.13396	-4292.62328	-4292.66507	-532.71059	-4517.20761	-4517.24577
E(BS5,SMD)	-3984.52978	-308.14039	-4292.65531	-4292.69708	-532.71305	-4517.23670	-4517.27394
Volume (PCM)	676.014	169.629	812.441	805.763	199.848	841.11	830.701
Volume (SMD)	596.953	119.961	694.664	688.556	188.151	751.718	739.144
PBE0D3(0)/BS1 optimized structures		ADC	TS ([**1**]$^+$,ADC)	Prod ([**1**]$^+$,ADC)	PrA	TS ([**1**]$^+$,PrA)	Prod ([**1**]$^+$,PrA)
E(BS1)		-453.97942	-2886.55014	-2886.58680	-191.63077	-2624.19076	-2624.23440
Thermal corr. to H (298 K)		0.06877	0.64835	0.65008	0.06714	0.64669	0.64964
Thermal corr. to G (298 K)		0.02644	0.52873	0.53264	0.03468	0.53532	0.54064
Standard State Corr.		0.00302	0.00302	0.00302	0.00302	0.00302	0.00302
Symmetry Corr.		0.00065	0.00000	0.00000	0.00065	0.00000	0.00000
E(BS2,PCM)		-454.14192	-2887.05096	-2887.08593	-191.70545	-2624.60250	-2624.64480
E(BS2,SMD)		-454.14522	-2887.08116	-2887.11570	-191.70839	-2624.63164	-2624.67360

E(BS5,PCM)		-454.18209	-4438.67894	-4438.71604	-191.71883	-4176.20471	-4176.24940
E(BS5,SMD)		-454.18529	-4438.70897	-4438.74565	-191.72171	-4176.23373	-4176.27784
Volume (PCM)		147.435	790.675	779.544	100.613	745.283	737.041
Volume (SMD)		161.211	725.791	713.058	82.659	651.937	647.603

Table S8. Computed energies (Hartrees) and vdW volumes (cm^3mol^{-1}) for the optimized structures associated with the study of $[Mo_3S_4(acac)_3(py)_3]^+$.

PBE0D3(0)/BS1 optimized structures	Cluster	TS with dmad	TS with ADC	BTD	TS with BTD	TS with PrA	Prod with PrA
E(BS1)	-2024.33856	-2556.84307	-2478.33156	-306.03754	-2330.38153	-2215.96924	-2216.01326
Thermal corr. to H (298 K)	0.68266	0.81107	0.75165	0.10384	0.78683	0.75027	0.75340
Thermal corr. to G (298 K)	0.54193	0.64341	0.59096	0.06304	0.62799	0.59667	0.60443
Standard State Corr.	0.00302	0.00302	0.00302	0.00302	0.00302	0.00302	0.00302
Symmetry Corr.	0.00104	0.00000	0.00000	0.00065	0.00000	0.00000	0.00000
E(BS5,PCM)	-3576.53174	-4109.24032	-4030.71161	-306.17799	-3882.69759	-3768.23510	-3768.27834
E(BS5,SMD)	-3576.56408	-4109.27153	-4030.74438	-306.18303	-3882.73065	-3768.26718	-3768.31019
Volume (PCM)	921.412	1090.019	1036.424	139.814	1031.521	997.456	988.043
Volume (SMD)	764.552	915.838	890.658	123.17	861.253	820.436	815.999
PBE0D3(0)/BS1 optimized structures	TS with PhA	Prod with PhA	^{F}PhA	TS with ^{F}PhA	^{CF3}PhA	TS with ^{CF3}PhA	
E(BS1)	-2332.36647	-2332.40460	-407.17112	-2431.51080	-981.47931	-3005.82816	
Thermal corr. to H (298 K)	0.80086	0.80387	0.11043	0.79348	0.13508	0.81816	
Thermal corr. to G (298 K)	0.64531	0.64970	0.07059	0.63592	0.07702	0.64608	
Standard State Corr.	0.00302	0.00302	0.00302	0.00302	0.00302	0.00302	
Symmetry Corr.	0.00000	0.00000	0.00065	0.00000	0.00065	0.00000	
E(BS5,PCM)	-3884.65503	-3884.69282	-407.32747	-3983.84868	-981.89460	-4558.41983	
E(BS5,SMD)	-3884.69060	-3884.72826	-407.33327	-3983.88326	-981.89902	-4558.45266	
Volume (PCM)	1059.482	1053.765	175.943	1065.045	259.638	1139.597	
Volume (SMD)	860.652	855.051	128.985	869.525	209.437	945.306	